Supporting Information

KB343, a cyclic *tris*-guanidine alkaloid from Palauan zoantharian *Epizoanthus illoricatus*

Ken Matsumura[†], Tohru Taniguchi[‡], James D. Reimer[¶], Shuntaro Noguchi[†], Masaki J. Fujita[†], and Ryuichi Sakai[†]*

†Faculty and Graduate School of Fisheries Sciences, Hokkaido University, 3-1-1 Minato-cho, Hakodate, Hokkaido 041-8611, Japan,
‡Frontier Research Center for Advanced Material and Life Science, Faculty of Advanced Life Science, Hokkaido University, Kita 21 Nishi 11, Sapporo 001-0021, Japan
¶University of the Ryukyus Senbaru 1, Nishihara, Okinawa 903-0213, Japan

Table of Contents

1. Supporting results

1.1. NMR assignments for **1**.

Detailed analyses of ^{1}H and ^{13}C NMR data for **1** was made from the 1- and 2D NMR data taken in both D_2O and acetonitrile-d_3. ^{15}N NMR and ^{1}H-^{15}N HMBC data were taken in acetonitrile-d_3

Table S1. NMR Data (400MHz, D_2O) for KB 344 (1).

position	δ_C	δ_H mult. (*J* in Hz)	COSY	HMBC	NOESY
1	188.2, C				
2α	40.5, CH_2	2.71, m	3	1, 3, 4, 8, 10	4α, 4β
2β		2.69, m	3	1, 3, 4, 8, 10	3, 4α, 4β
3	40.0, CH	2.87, dddd (12.4, 9.1, 6.9, 3.3)	2, 4	1, 4, 5, 8, 9 (w)	2β, 4β, 5, 7
4α	29.7, CH_2	1.53, dt (14.4, 12.4)	3, 4β, 5	3, 5, 6, 8, 11	2, 4β, 11
4β		1.63, dt (14.4, 3.3)	3, 4α, 5	3, 5, 6, 8, 11	2, 3, 4α, 5, 11
5	38.6, CH	1.90, ddq (12.4, 3.3, 6.7)	4α, 4β, 11	3, 4, 11	3, 4β, 7, 11, 12β
6	69.0, C				
7	63.9, CH	4.33, s		6, 8, 9, 12, 14	3, 5, 12α
8	63.3, C				
9	143.8, C				
10	122.9, C				
11	14.3, CH_3	1.02, d (6.7)		4, 5, 6	4α, 4β, 5, 12β
12α	52.7, CH_2	3.71, d (11.3)	12β	5, 6, 7, 13	7, 12β
12β		3.83, d (11.3)	12α	5, 6, 7, 13	5, 11, 12α
13	160.5, C				
14	161.9, C				
15	151.0, C				

Taken in D_2O with addition of CD_3OD-d_4 as internal standard (δ_H 3.30, δ_C 49.0 ppm). Measured at 303 °K.

Table S2. NMR Data (400MHz, CD_3CN at 298 °K) for 1.

position	δ_C	δ_N	δ_H mult. (*J* in Hz)	COSY	HMBC (^{13}C and ^{15}N)	NOESY
1	185.8, C					
2α	41.1, CH_2		2.62, dd (16.8, 12.0)	3	1, 3, 4, 8, 10	4
2β			2.49, dd (16.8, 2.8)		1, 3, 4, 8, 10	3, 4
3	40.7, CH		2.71, m	2, 4	1, 4	2β, 4, 5, 7
4	30.2, CH_2		1.49, m	3, 5	6, 8	2, 3, 11, 1'
5	38.9, CH		1.80, m	4, 11	3, 4, 6, 11, 12(w) [a]	3, 7, 11, 12b
6	68.7, C					
7	63.8, CH		4.12, s	4', 6'	6, 8, 9, 12, 14, 1', 6'	3, 5, 12α, 4'
8	63.2, C					
9	144.8, C					
10	123.0, C					
11	14.9, CH_3		0.96, d (6.8)		4, 5, 6	4, 5, 12β, 1'
12α	53.2, CH_2		3.57, d (10.8)	12b, 1', 3'	5, 6, 7, 13	
12β			3.68, d (10.8)	12a, 1', 3'		
13	161.2, C					
14	162.3, C					
15	152.6, C					
1'		82.9, N	8.13, s	12a, 12b, 3'	6, 12, 13, 3'	4, 11
3'		75.6, N	7.87, s	12a, 12b, 1'	6, 12, 13, 1'	12α, 12β
4'		86.2, N	9.38, s	7, 6'	8, 14	7
6'		92.5, N	9.81, s	7, 4'	7, 14	

[a] w: weak signal.

1.2. Structure of the alcohol **5**.

The molecular formula for **5**, $C_{15}H_{24}N_9O$, was secured by its HRESIMS together with the ^{13}C NMR data which showed all 15 carbon atoms (Table S3). Loss of the carbonyl group was evident as an absorption as UV absorptions at λ 310 nm and IR absorption at 1658 cm^{-1} were lost. ^{1}H and ^{13}C NMR data for **5** were assigned using 2D NMR experiments confirming the carbon-nitrogen framework for **5** was the same as that of **1**. However, a new spin system for a secondary alcohol δ_H 4.81/δ_C 62.1 appeared for C-1 of **5** confirmed that **5** is a 1-ol derivative of **1**. Coupling constants, 9.3 and 6.9 Hz for the oxymethine at δ_H 4.81 and NOESY correlation between H-1 and H-2b or H-3 indicated that it is β-axial. A loss of H_2O was observed in MS/MS spectrum, supporting the presence of alcohol in **5**.

Table S3. NMR Data (400 MHz, D_2O, at 303 °K) for alcohol 5.

position	δ_C	δ_H mult. (*J* in Hz)	COSY	HMBC	NOESY
1	62.1, CH	4.81, dd (9.3, 6.9)	2α, 2β [α]	2(w), 9 (w), 10	2β (or 3)
2α	35.0, CH_2	1.63, dt (9.3, 13.5)	1, 2β, 3 [α]	1	2β (or 3)
2β		2.22, m	1, 2α, 4α, 4β [α]	1, 8, 10 [α]	1, 2α, 4β, 5, 7 [a]
3	38.0, CH	2.24, m			
4α	29.4, CH_2	1.39, dt (14.3, 12.3)	3, 5	6 (w) [b]	4β, 11
4β		1.52, dt (14.3, 3.3)	3, 5	6 (w), 8 (w)	3 (or 2β), 4α, 11
5	38.3, CH	1.79, m	4α, 4β, 11		3 (or 2β), 4β, 7, 11, 12β
6	68.1, C				
7	63.7, CH	4.07, s		6(w), 8, 9, 12, 14	3 (or 2β), 5, 12α
8	62.7, C				
9	123.7, C				
10	125.6, C				
11	13.5, CH_3	0.94, d (6.8)	5	4, 5, 6	4α (w), 4β, 5, 12β
12α	52.0, CH_2	3.60, d (11.2)	12β	5, 6, 7, 13	7, 12β
12β		3.74, d (11.2)	12α	5, 6, 7, 13	5, 11, 12α
13	159.6, C				
14	160.9, C				
15	147.9, C				

[a] signals for 2β and 3 are overlapped. [b] w : weak signal.

1.3. Structure of the monopyrimidine **2**.

The molecular formula for **2**, $C_{20}H_{25}N_9O$, was secured by its HRESIMS. Analysis of NMR data established the same spin systems as those of **1**, except that C-9 and C-10 atoms were not observed in the ^{13}C NMR. Nevertheless, the skeletal structure of **2** was secured on the basis of correlation spectral data (Table S4). The newly added groups: two methyl singlets, aromatic methane, and aromatic quaternary carbons were assigned for a dimethylpyrimidine group. Because four NH's for two aminoimidazoline systems were found intact, the diketone must be reacted to the N-8' and N-9' or N-7 and N-9 to form pyrimidinium group to form possible derivatives A or B. Computer modeling with molecular dynamics and energy minimization (MM2) calculation on ChemDraw of two possible products indicated that the former one (A) is more favorable (32 Kcal/mol) than the latter (B, 49 Kcal/mol). We thus concluded that the pyrimidine was formed with the nitrogen atoms N-8' and -9' (Figure S1).

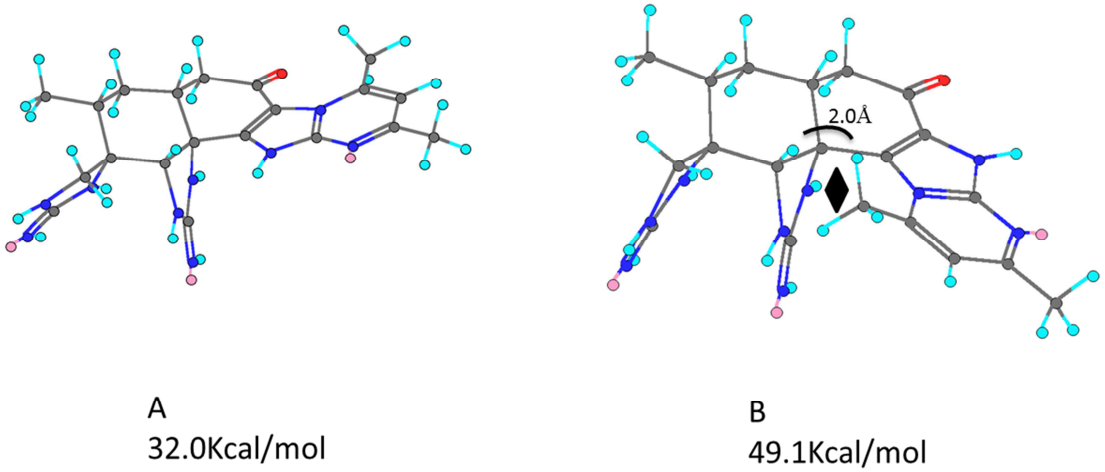

Figure S1. Computer generated models for possible structures for monopyrimidine **2**. Model B has severe steric collision between the methyl group of the pyrimidine and the guanidine group in the middle (black diamond).

Table S4. NMR Data (400 MHz, CD_3CN at 298 ^oK) for monopyrimidine derivative 2.

position	δ_C	δ_H mult. (*J* in Hz)	COSY	HMBC	NOESY
1	184.2, C				
2α	42.6, CH_2	2.78, m	2β, 3	3	
2β		2.65, m	2α, 3	1, 3, 8	
3	39.3, CH	2.74, m			4β, 5, 7
4α	30.5, CH_2	1.53, dt (14.4, 11.4)	3, 4β, 5		4β, 11, 1'
4β		1.70, dt (14.4, 3.8)	3, 4α, 5	3	2β, 3, 4α, 5, 11
5	37.8, CH	1.97, m	4α, 4β, 11		3, 4β, 7, 11, 12β
6	68.5, C				
7	64.5, CH	4.48, s		8, 12, 14	3, 5, 12α, 1' (w), 4' (w)
8	64.3, C				
9	not observed				
10	not observed				
11	15.8, CH_3	1.03, d (6.8)		4, 5, 6	4α, 4β, 5, 12β, 1'
12α	53.9, CH_2	3.63, d (10.8)		5, 6, 7, 13	7, 3' (w)
12β		3.69, d (10.8)			5, 11, 3' (w)
13	161.2, C				
14	161.6, C				
15	153.6, C				
1'		8.40, s		6 (w) [c], 12, 13	4α, 7 (w), 11
3'		8,45, s			12α (w), 12β (w)
4'		9.68, s			7 (w)
6'		10.20, s			
6''	24.7, CH_3 [a]	2.55, s [a]		7'', 8''	8''
7''	166.9, C [b]				
8''	114.6, CH	6.95, s	10''	7'', 9'', 10''	6'', 10''
9''	151.2, C [b]				
10''	22.8, CH_3 [a]	2.92, s [a]	8''	8'', 9''	8''

[a, b] Signals are interchangeable. [c] w : weak signal.

1.4. Structure of the bispyrimidine **3**.

In the ESIMS spectrum, both single and doubly charged ions were observed. The formula for **3**, $C_{25}H_{29}N_9O$ was established from both $m/z = [M + H]^+$ and $m/2z = [M + 2H]^+$ data. Detailed analyses for the 1- and 2D NMR for **3** allowed to assign all signals, but missing C-9 (Table S5). Besides the substructure for **1**, **3** contained 10 additional carbon atoms for two newly formed dimethyl pyrimidines (C-1”—C—5” and C-6”—C—10”). The position of the second pyrimidine unit was confirmed to be in N2’—C13’—N3’ face because of an NOESY correlation between H−1” and H-12 (Figure S2). Of note, an unusual downfield shift for C4” was observed. Although the reason for this is not clear, the correlation NMR data was consistent with the assignment (Figure S2, S3).

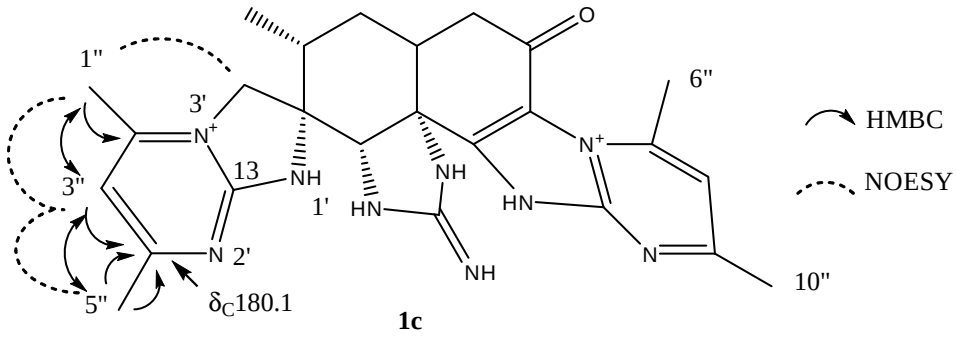

1c

Figure S2. The structure of bispyrimidine **3.**

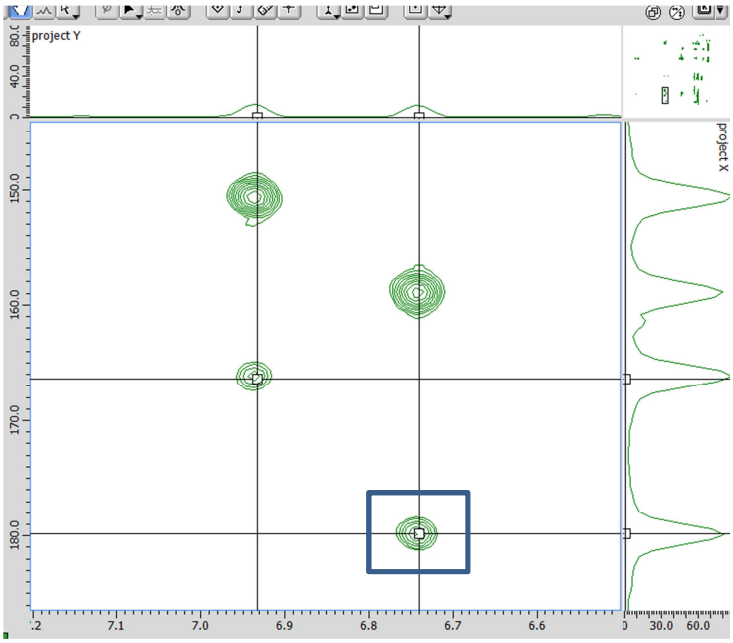

Figure S3. HMBC data (zoomed) for **3** showing a correlation between H3” and C4 (box).

Table S5. NMR Data (400 MHz, CD_3CN at 298 ^oK) for bispyrimidine derivative 3.

position	δ_C	δ_H mult. (*J* in Hz)	COSY	HMBC	NOESY
1	184.2, C				
2α	42.6, CH_2	2.85, dd (16.4, 12.4)	2β, 3	1, 3, 8	2β, 4α
2β		2.66, dd (16.4, 3.2)	2α, 3	1, 3, 8, 10	2α, 4β, 11
3	39.6, CH	2.75, tt (12.2, 3.4)	2, 4α, 4β		4β, 5, 7, 12
4α	30.6, CH_2	1.64, dt (14.4, 11.6)	3, 5	3, 5, 6, 8	2α, 4β, 11
4β		1.77, dt (14.4, 4.0)	3, 5	3, 5, 6, 8	2β, 3, 4α, 5, 11
5	37.7, CH	2.12, m	4, 11		3, 4β, 7, 11, 12
6	67.1, C				
7	65.7, CH	4.70, brs		8, 12, 14	3, 5, 12, 4'
8	64.1, C				
9	not observed				
10	119.1, C				
11	16.2, CH_3	1.06, d (6.8)		4α, 4β, 5, 6	4α, 4β, 5, 12
12	57.2, CH_2	4.53, brs		5, 7, 13	3, 5, 7, 11, 1"
13	158.5, C				
14	161.6, C				
15	153.7, C				
4' NH		10.90, brs		8, 14 (w) [c]	7
6' NH		10.52, brs		7, 14(vw) [d]	
1"	18.7, CH_3	2.41, s	3"	2", 3"	3", 12
2"	159.2, C				
3"	112.7, CH	6.75, s	1"	1", 2", 4", 5"	1", 5"
4"	180.1, C				
5"	25.4, CH_3	2.43, s		3", 4"	3"
6"	24.7, CH_3 [a]	2.54, s [a]		7", 8"	8"
7"	166.4, C [b]				
8"	114.4, CH	6.94, s	10"	7", 9", 10"	6", 10"
9"	150.9, C [b]				
10"	22.8, CH_3 [a]	2.93, s [a]	8"	8", 9"	8"

[a, b] Signals are interchangeable. [c] w : weak signal. [d] vw : very weak signal.

1.5. Determination of the absolute configuration

Experimental CD spectra of **1** and **5** were recorded on a JASCO J-725S spectrometer using a 1-mm quartz cell. The raw CD spectra were corrected using a solvent (water) spectrum obtained under the identical measurement conditions. The resultant CD spectra were presented as Δε (in M^{-1} cm^{-1}, see experimental section).

Theoretical calculations of CD spectra started with a preliminary MMFF conformational search of arbitrarily chosen (3*R*,5*R*,6*S*,7*R*,8*S*)-**1** and (1*S*,3*R*,5*R*,6*S*,7*R*,8*S*)-**5** on CONFLEX 7 software.[1] The obtained geometries within 10 kcal/mol from the most stable were further optimized by DFT using the B3LYP functional and the 6-31G(d) basis set with the polarizable continuum model (PCM) for water using Gaussian09.[2] This resulted in only 2 stable conformers in a 2 kcal/mol energy window for each **1** and **5** (Figure S4). The CD and UV spectra of the resultant stable conformers were calculated at the same level of theory, where the first 40 singlet → singlet electronic transitions were taken into account. Calculated CD and UV spectra were simulated using Gaussian band shapes with 0.333 eV half-width at half height. The calculated wavelengths were manually shifted to longer wavelength by 15 cm^{-1}. The final spectra were obtained by weighted-average of the spectra for each conformer on the basis of its Boltzmann populations.

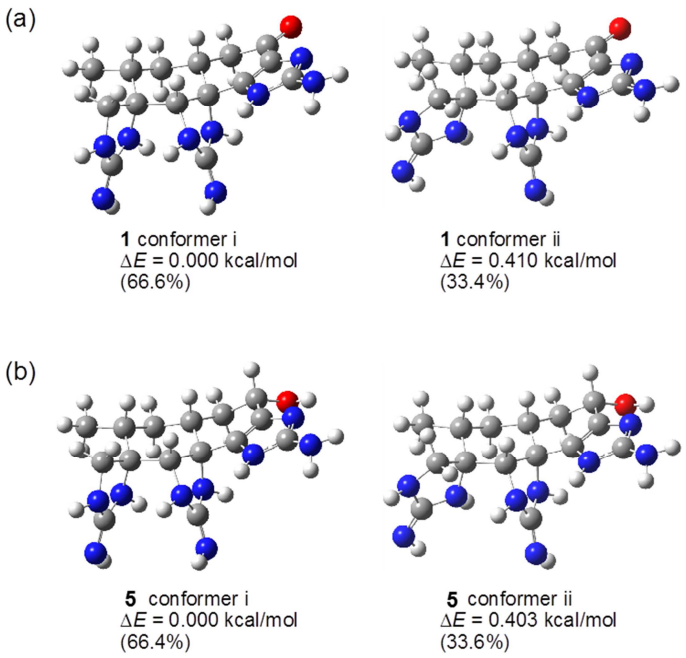

Figure S4. Stable conformers of (a) **1** and (b) **5** predicted using DFT optimization at B3LYP/6-31G(d)/PCM (water).

The 3*R*,5*R*,6*S*,7*R*,8*S* absolute stereochemistry assigned for **1** was further supported by CD studies on **5**. The observed CD data for a water solution of **5** was compared with the theoretical spectrum for (1*S*,3*R*,5*R*,6*S*,7*R*,8*S*)-**1** calculated at the DFT/B3LYP/6-31G(d)/PCM (water) level (Figure S5). The experimental CD spectrum showed a broad positive Cotton effect below 250 nm. This feature was also seen in the calculated CD spectrum, despite the separation of the calculated positive signal into two bands. This result suggested the absolute stereochemistry of **5** to be 1*S*,3*R*,5*R*,6*S*,7*R*,8*S* and that of its precursor **1** to be 3*R*,5*R*,6*S*,7*R*,8*S*.

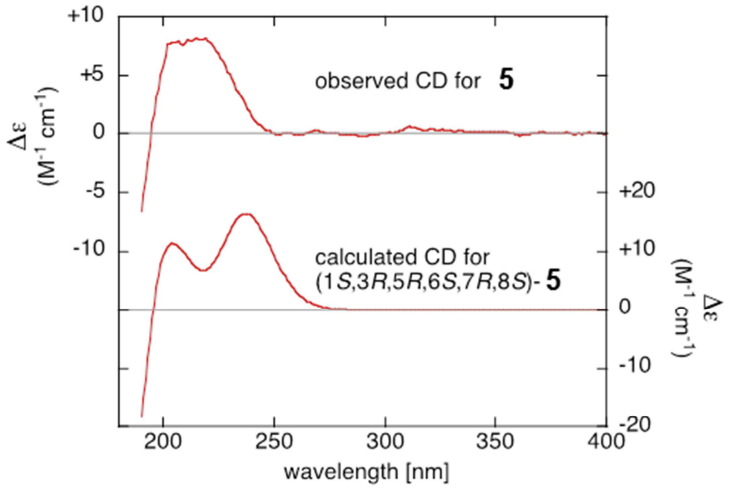

Figure S5. Comparison between the CD spectrum observed for **5** and that calculated for (1*S*,3*R*,5*R*,6*S*,7*R*,8*S*)-**5**. Measurement conditions: *c* = 0.29 mM in water. Calculation conditions: DFT/B3LYP/6-31G(d)/PCM (water).

1.6. Excited state calculations

The DFT spectral calculations of **1** and **5** also predicted the lower-energy excitation states responsible for the UV absorption bands in the longer-wavelength region. As for **1**, the absorption band at around 307 nm was mainly ascribed to the HOMO → LUMO transition (the second excited state S_2) (Figure S6 and S7). DFT optimization of the excited state S_2 at the B3LYP/6-31G(d)/PCM (water) level yielded a geometry whose conjugation character around the α,β-unsaturated ketone is slightly different from the ground state (Figure S6d). The energy difference between the optimized state S2 and the ground state (3.45 eV) is in good agreement with the observed fluorescence between 369 and 500 nm, centered at 421 nm.

(a)

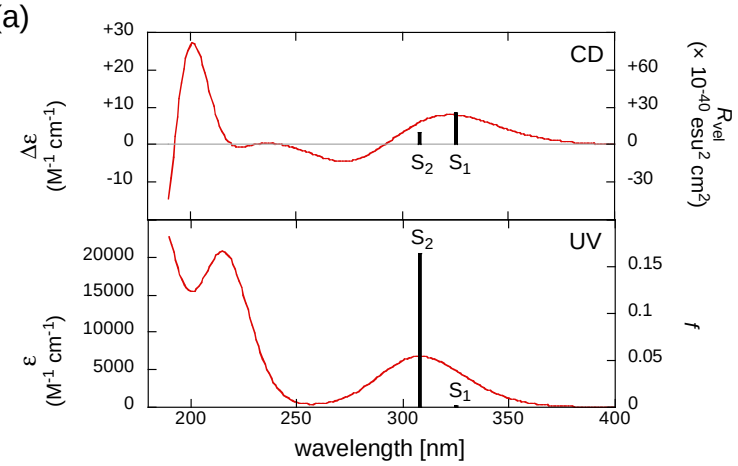

(b)

State	Excitation	*f*
S_1	HOMO-3 → LUMO HOMO-4 → LUMO	0.0013
S_2	HOMO → LUMO	0.1646

(c)

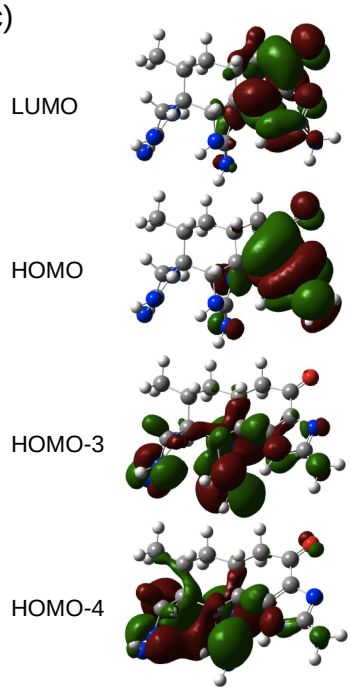

(d)

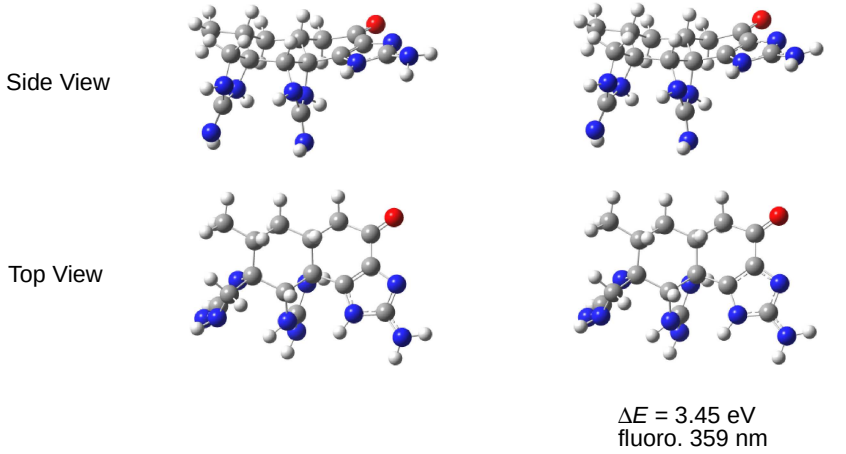

Figure S6. The two lowest-energy transitions of **1** calculated at DFT/B3LYP/6-31G(d)/PCM (water). R_{vel}: rotatory strength in velocity form. *f*: oscillator strength. (a) Calculated CD and UV spectra and the two lowest-energy transitions of **1**. (b) The excitation and oscillator strength (*f*) of the two lowest-energy transitions S_1 and S_2. (c) Schematic molecular orbitals involved in the states S_1 and S_2. (d) Comparison of the ground state and the optimized excited state S_2 of **1**. The difference in their energies is also shown.

(a)

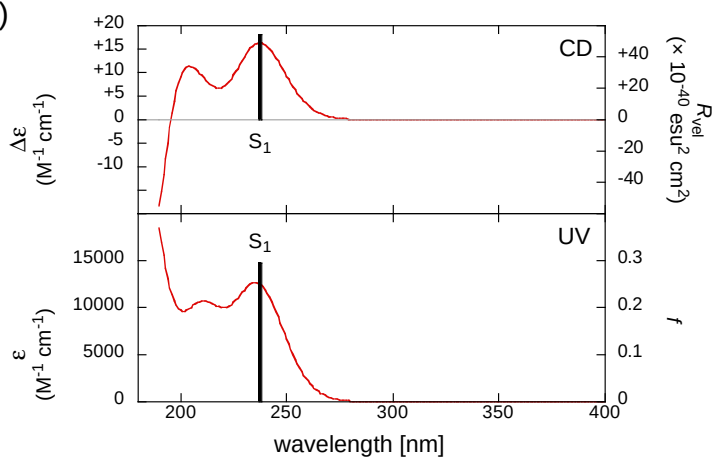

(b)

State	Excitation	*f*
S_1	HOMO → LUMO+1 HOMO → LUMO	0.2950

(c)

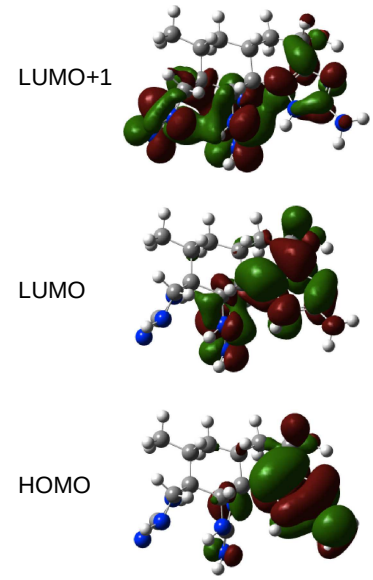

Figure S7. The lowest-energy transition of **5** calculated at DFT/B3LYP/6-31G(d)/PCM (water). R_{vel}: rotatory strength in velocity form. *f*: oscillator strength. (a) Calculated CD and UV spectra and the lowest-energy transition of **5**. (b) The excitation and oscillator strength (*f*) of the lowest-energy transition S_1. (c) Schematic molecular orbitals involved in the state S_1.

1.7. Evaluation of cytotoxicity

Cytotoxicity of KB 343 (**1**) and its derivatives (**5**, **2** and **3**) were evaluated by using L1210, HeLa and SH-SY5Y cells. IC_{50} values were determined on the basis of concentration response curves (Figure S8). IC_{50} values of compound **1**, **5**, **2**, **3** for L1210 cells in μM was each 1.96 [n=5, 95% confidence interval (CI) = 1.66~2.33]; 5.01 (n=5, 95% CI = 4.40~5.71); 0.38 (n=5, 95% CI = 0.34~0.42); and >500, respectively. Those for HeLa cell of compound **1**, **5**, **2** was each 4.93 [n=5, 95% CI = 4.67~5.21]; >100 (n = 5); 23.1 (n=5, 95% CI = 21.2~26.4), respectively. Compound **3** was not active. Those of compound **1**, **5**, **2**, **3** for SH-SY5Y cells was each 3.40 [n = 5, 95% CI = 2.84~4.07]; 10.9 (n = 5, 95% CI = 8.57~13.97); 5.11 (n = 5, 95% CI = 2.28~3.19); and >300, respectively.

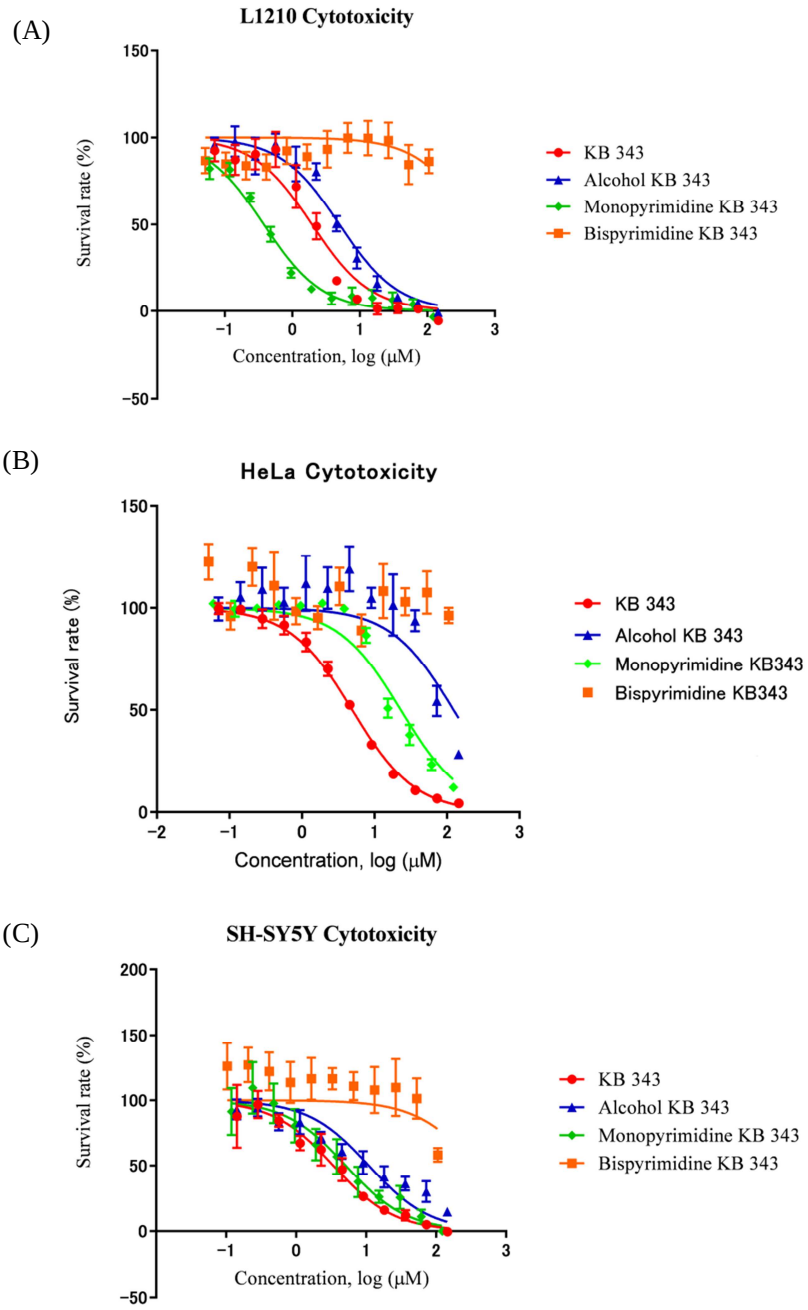

Figure S8. Cytotoxicity against (A) L1210, (B) HeLa, (C) SH-SY5Y cells for KB343 (**1**), alcohol derivative (**5**), monopyrimidine derivative (**2**), and bispyrimidine derivative (**3**).

2. Experimental Section

2.1. General Procedure

NMR data were obtained on a JEOL ECZS400 spectrometer. Samples were dissolved either in deuterium oxide (99.990 atom %D) or acetonitrile-d_3 (99.9 atom % D). ^{1}H chemical shifts were referenced to residual signals of D_2O and acetonitrile-d_3 at δ 4.65 and 1.93, respectively. ^{13}C-NMR chemical shifts were referenced to acetonitrile-d_3 solvent peak at δ 1.30. The infrared spectra were measured using KBr pellet on a JASCO FT-IR 4200. Optical rotation was obtained on a JASCO 2200 polarimeter using 3 x 10 cm cell, and the α value was adjusted against water blank. MALDI-TOF MS was measured on an AB4700 spectrometer using either α-cyano-4-hydroxycinamic acid (CHCA) or gentisic acid (GA) as a matrix. The Q-TOF LC HIRESMS experiments were performed in a positive ESI mode on a Sciex 5600 system in an infusion mode with collision energy of 25V. HPLC was performed on a system comprised of a pump LC-20AD and a photodiodearray detector SPD-M20A (Shimadzu) using a COSMOSIL (5C18-AR-II Packed Column, 10 mm I.D. × 250 mm), eluting with a gradient of MeOH- H_2O both containing 0.05% trifluoroacetic acid (v/v).

2.2. Animal Material

A sample of the zoantharian was collected at Republic of Palau in 2007 (Siaes Tunnel, Pal 448) by using SCUBA at a depth of 20 m. The specimen stored in 70% ethanol was identified by J.R. The species was identified as *Epizoanthus* by its association with zig-zag eunicid worms, and its external coloration and habitat were used to distinguish the species from its closely related congener *E. beriber*, described from Palau, which is white in color[1]

2.3. Biological assays

The mouse behavioral assays were performed under approval by the Ethical Committee of Experimental Animal Care at Hokkaido University. The effects of samples on mice behaviors were assessed as described previously.[2] Briefly, an aqueous solution of sample (10 μL) was injected intracerebroventricularly (i.c.v.) in male ddY mice of 3 to 4 weeks (Japan SLC Inc, Hamamatsu). Mouse behavior was observed for 1 h. for acute behaviors such as convulsion. The survived individuals were observed once a day for one month, and numbers of mice died were recorded.

Antifungal assay against *Saccharomyces cerevisiae* was conducted using baker's dry yeast (Nisshin Seifun). Pre-cultured yeast in YPD media was inoculated (0.3 mL) to agar plate at 1.2×10^7 CFU/mL. Test compound was applied on a 0.6 mm paper disc and incubated at 37 ^{o}C for 18 h. Filipin was used as positive control (7.6 mm inhibition zone at 5 μg/disc). The concentration that showed minimum observable inhibition was defined as minimum inhibitory concentration (MIC).

2.4. Cell culture

L1210 (Riken RBRC-RCB2844), HeLa (RBRC-RCB0007), and SH-SY5Y cells (ATCC CRL-2266) were used. Culture media used for each L1210, HeLa, and SH-SY5Y cells was RPM1640, EMEM, and DMEM/Ham's F-12, respectively, with 10% FBS for all the media (Wako Pure chemicals, Osaka). Cells were pre-cultured using CO_2 incubator (37 ^{o}C, 5% CO_2) for 3 days (L1210, HeLa) or 7 days (SH-SY5Y). For L1210, confluent cells (1×10^5 cells/mL) were inoculated (50 μL) to each well of 98-well microtiter plate. The sample dissolved in the medium (200 μg/mL) was filtered (0.22 μm) and

serially diluted, and then added (50 μL) to each well so that the final concentration of sample between 50 and 0.024 μg/mL, and cell 5000 cells/well, were archived. For HeLa and SH-SY5Y, confluent cells (each 2 x 104 cells/mL for HeLa; or 5 x 104 cells/mL) were inoculated (100 μL) to the well and pre-incubated for 24 h. Sample (10 μL) was added to the well (final concentration of sample 50-0.024 μg/mL) and incubated for 48 h. Growth of cells was quantified using cell counting kit-8 (WST-8, Dojindo Laboratories, Kumamoto) following manufacturer's protocol. Absorption at 450 nm was measured using microplate reader. Mean triplicate of the data was plotted to generate concentration-response curve and was analyzed using Prism software (GraphPad).

2.5. Isolation of **1**.

A sample of Palauan specimen of zoantharian *E. illoricatus* (Pal 448, 175 g) was extracted with water and the aqueous extract was lyophilized to give a crude extract (6.8 g). The aqueous extract was dialyzed using a cellulose tube (40-50 Å pore) against water and the small molecular portion that passed through the membrane was lyophilized to give an extract (5.72 g). The extract was separated by a Sephadex LH-20 column (6 × 70 cm, 0.05% aqueous TFA, 1 mL/min, 10 mL/tube) and tubes were combined according to TLC and MALDI-TOFMS profile into a total of 10 fractions (TL1-27-1~10). Fraction 6 (TL1-27-6, 800 and 900 mL eluate, 301 mg) caused slow death (2 days) in mice, whereas Fraction 7 (100 mg) exhibited running behavior accompanying slow death (2 days). Since precipitation formed when TL1-27-6 was re-dissolved in water, it was filtered out and the lyophilized material (265 mg) was applied on a C18 reversed-phase open column using a step gradient elution of water (0.05% TFA) and methanol into 9 fractions (TL1-35-1~9). Fractions 3 and 4 showed the mice slow death activity. A part of the fraction 3 was purified by an HPLC (Inertsil ODS-3, 10 x 250 mm, 1.35 mL/min, water-0.05% TFA gradient). This separation was repeated to give pure **1** (27 mg) as trifluoroacetate.

KB 343 (**1**): White powder, $[\alpha]_D^{20}$ = +108.9 (*c* = 0.089, H_2O); UV (MeOH) λ_{max} (logε) 307 (3.86) nm; CD (H_2O) λ_{ext} 205 (Δε +16.3), 287 (-3.76), 318 (+8.05); IR (KBr) ν_{max} 3428, 2923, 2855, 1687, 1439, 1198, 1137, 1070 cm^{-1}; ^{1}H- and ^{13}C NMR (400 MHz, CD_3CN-d_3 or D_2O/CD_3OD-d_4 were shown in S1, and S2 respectively; HRESIMS: *m*/*z* 344.1942 $[M + H]^+$ (calcd for $C_{15}H_{22}N_9O$, *m*/*z* 344.1942).

2.6. $NaBH_4$ reduction of **1**.

KB 343 (**1**, 3 mg, 0.088 mmol) was dissolved in water. To the solution an excess amount of $NaBH_4$ was added and stood in room temperature for 30 min. The product was purified by HPLC as described above to afford 2.55 mg of the alcohol (**5**, white powder, 0.074 mmol, 84%): $[\alpha]_D^{20}$ = +103.3 (*c* = 0.01, H_2O); UV (MeOH) λ_{max} (logε) 220 (3.84) nm; CD (H_2O) λ_{ext} 214 br (Δε +7.73); IR (KBr) ν_{max} 3398, 2968, 1658, 1545, 1454, 1387, 1108 cm^{-1}; ^{1}H- and ^{13}C NMR (400 MHz, D_2O) shown in Table S3; HRESIMS: *m*/*z* 346.2103 $[M + H]^+$ (calcd for $C_{15}H_{24}N_9O$, *m*/*z* 346.2098).

2.7. Treatment of **1** with 2,4-pentanedione.

KB343 (3.9 mg, 0.011 mmol), 2,4-pentanedione (30 μL) and pyridine (200 μL) was heated at 75 ^oC for 3h. The product was purified on a HPLC as above to give **2** (0.91 mg, 0.0022 mmol, 20 %) and **3** (2.41 mg, 0.0051 mmol, 46%).

KB 343 monopyrimidine derivative (**2**): White powder, $[\alpha]_D$= +212; UV (c: 0.0326, H_2O) λ_{max} (logε) 211 (3.99), 254 (4.07), 311 (3.69) nm; IR (KBr) ν_{max} 3412, 3171, 1687, 1424, 1198, 1130 cm^{-1}; ^{1}H- and

^{13}C NMR (400 MHz, CD_3CN-d_3) shown in Table S4; HRESIMS: *m*/*z* 408.2252 $[M+H]^+$ (calcd for $C_{20}H_{26}N_9O$, *m*/*z* 408.2255).

KB343 bispyrimidine derivative (**3**): White powder, $[\alpha]_D$= +246.5; UV (c:0.0208, H_2O) λ_{max} (logε) 241 (4.26), 257 sh (4.22), 311 (3.97) nm; IR (KBr) ν_{max} 3436, 3164, 1688, 1409, 1183, 1130 cm^{-1}; ^{1}H- and ^{13}C NMR (400 MHz, CD_3CN-d_3) shown in Table S5; HRESIMS: *m*/*z* 472.2571 $[M+H]^+$ (calcd for $C_{25}H_{30}N_9O$, *m*/*z* 472.2568).

An LC-MS analysis of the product also showed a presence of trispyrimidine **4** along with **2** and **3**. Characterization of **4** with NMR was not possible due to a minute amount obtained while HRESIMS: *m*/*z* 536.2872 $[M+H]^+$ (calcd for $C_{25}H_{30}N_9O$, *m*/*z* 536.2881) was consistent with the expected formula.

3. Spectral Data

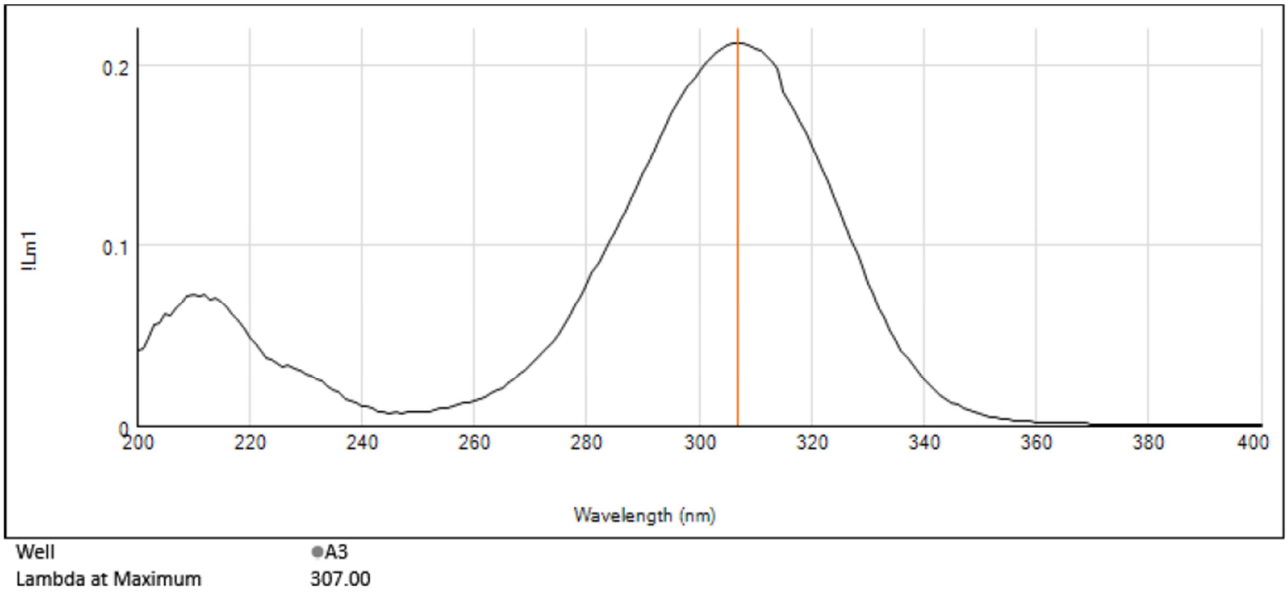

Figure S9. UV data for **1** in MeOH.

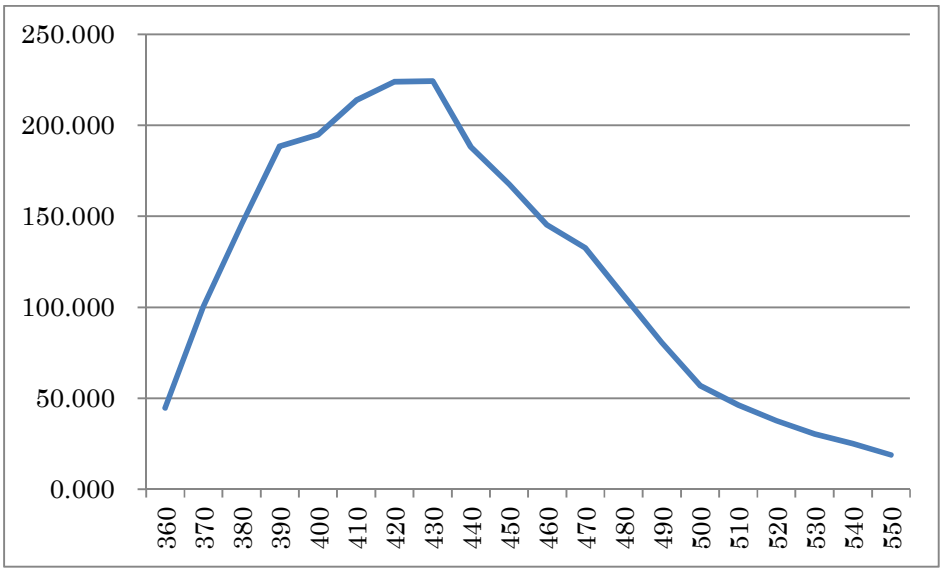

Figure S10. Fluorescent spectrum for **1** in H_2O (1 mg/mL)

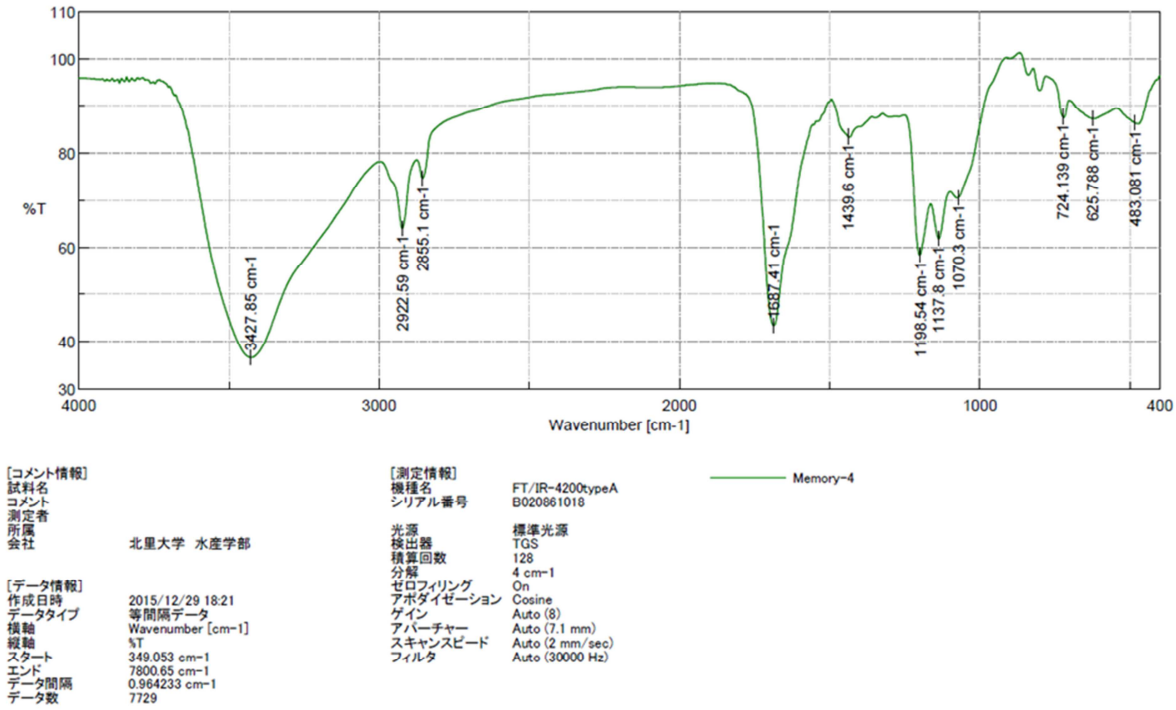

Figure S11. IR data (KBr) for **1**.

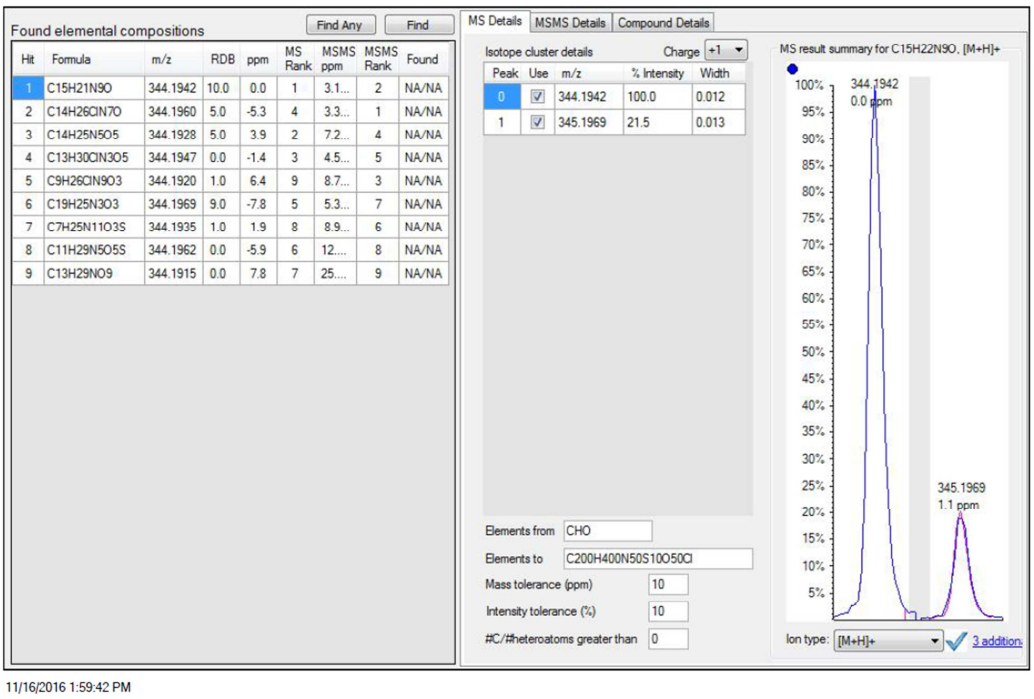

Figure S12. HRESIMS data for **1**.

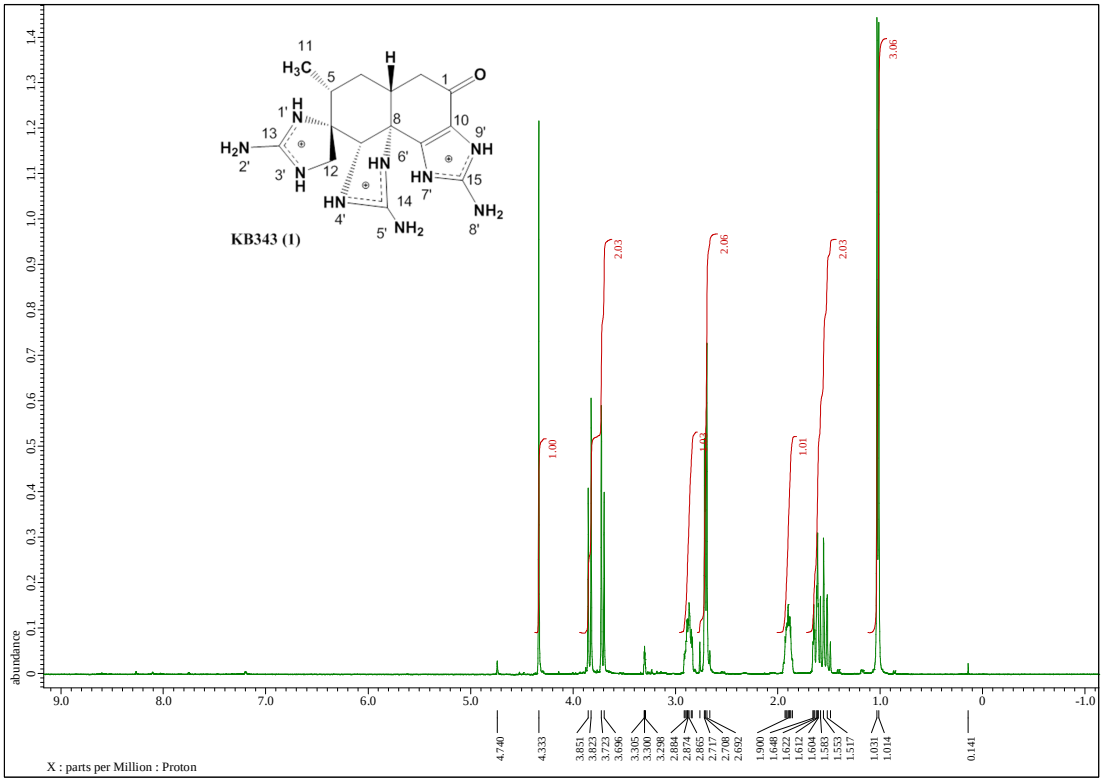

Figure S13. ^{1}H-NMR spectrum of **1** in D_2O with CD_3OD (400MHz).

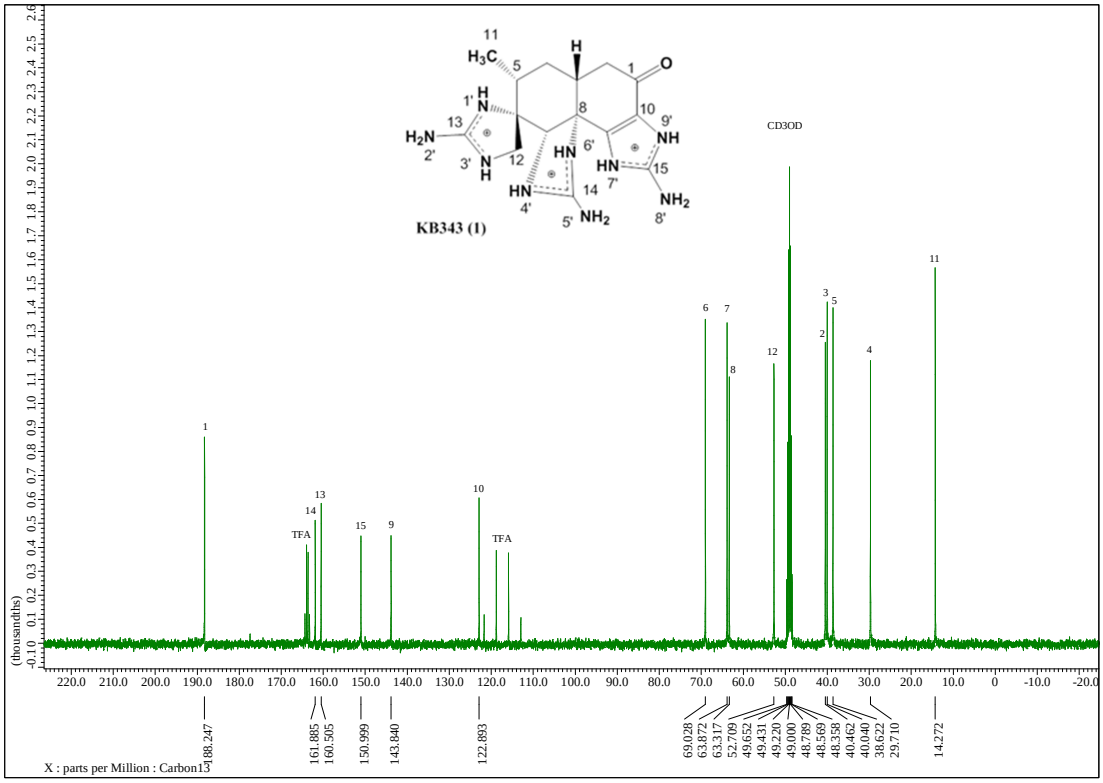

Figure S14. ^{13}C-NMR spectrum of **1** (TFA salt) in D_2O with CD_3OD (100 MHz).

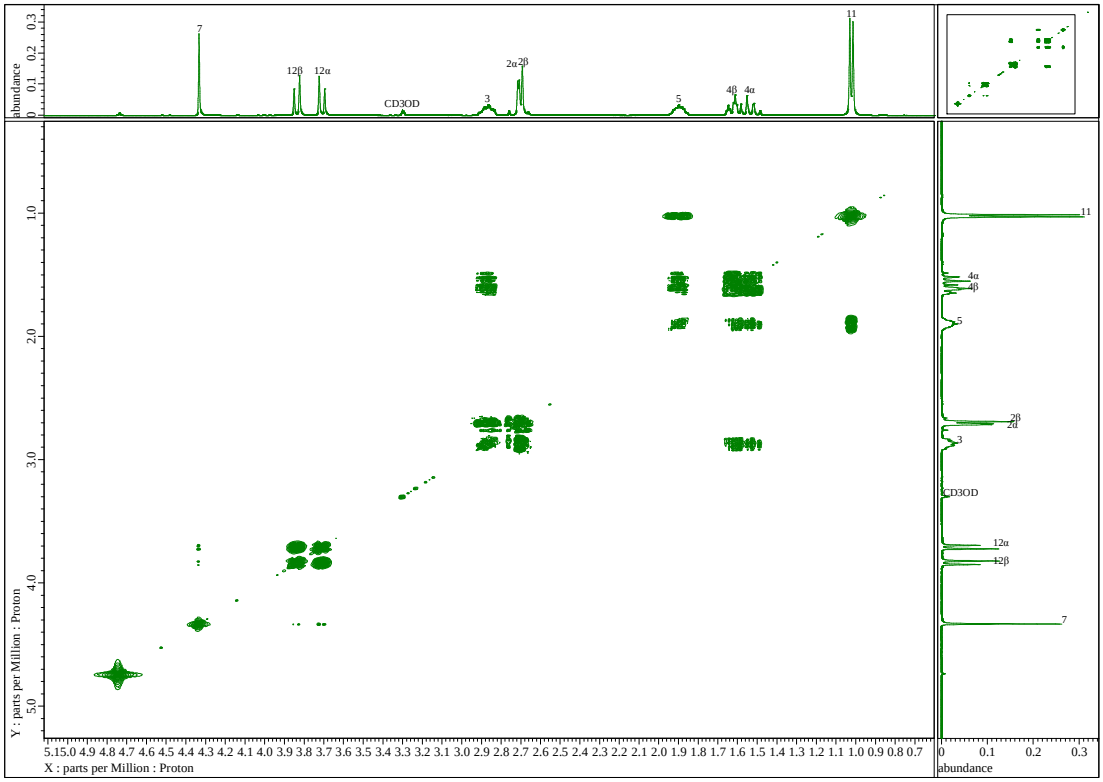

Figure S15. ^{1}H-^{1}H COSY spectrum of **1** in D_2O with CD_3OD (400MHz).

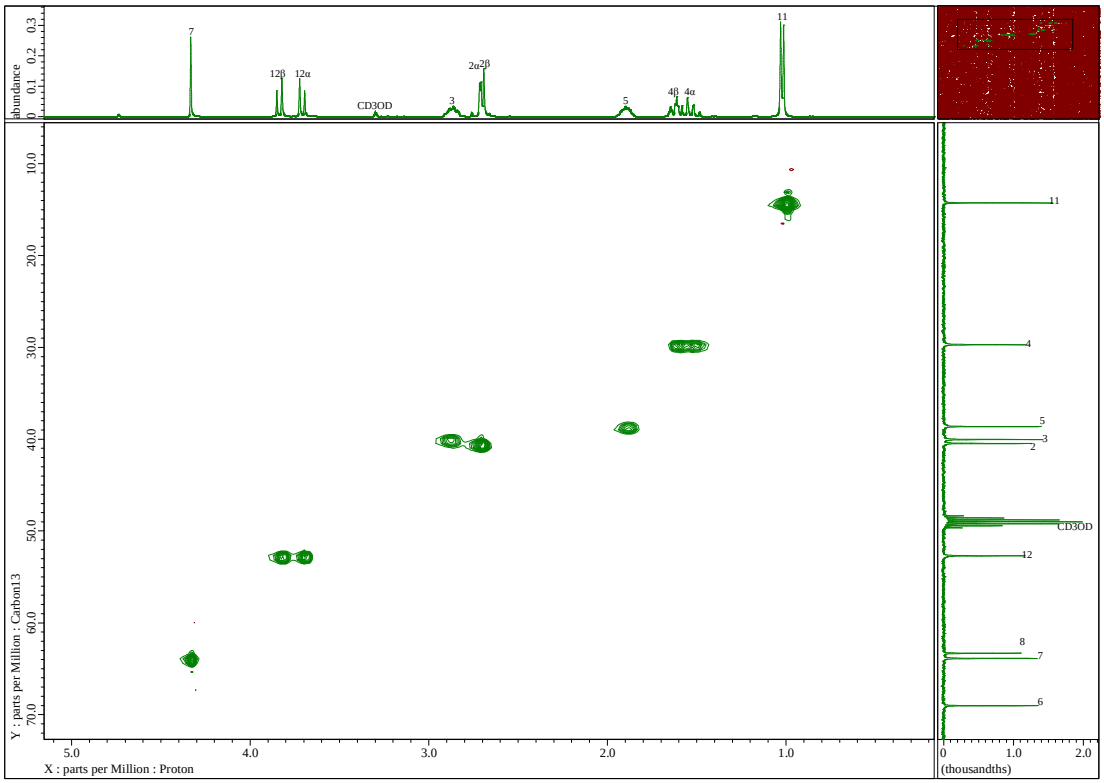

Figure S16. HSQC spectrum of **1** in D_2O with CD_3OD (400MHz).

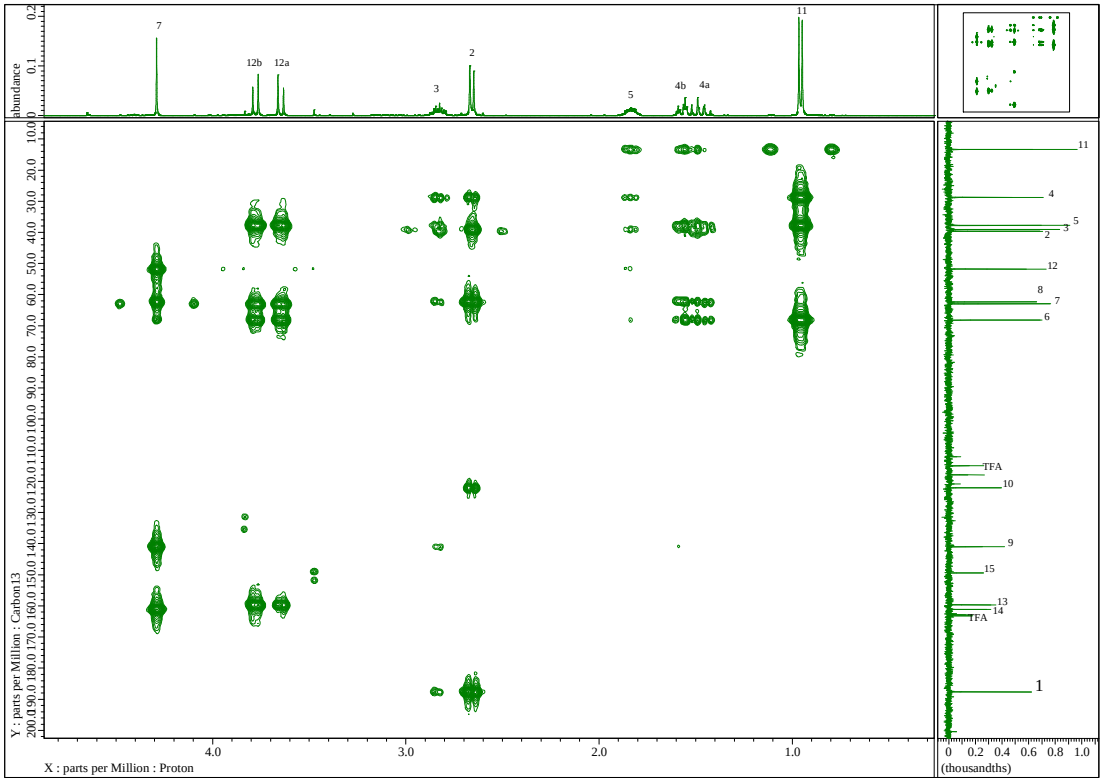

Figure S17. HMBC spectrum of **1** in D_2O (400MHz).

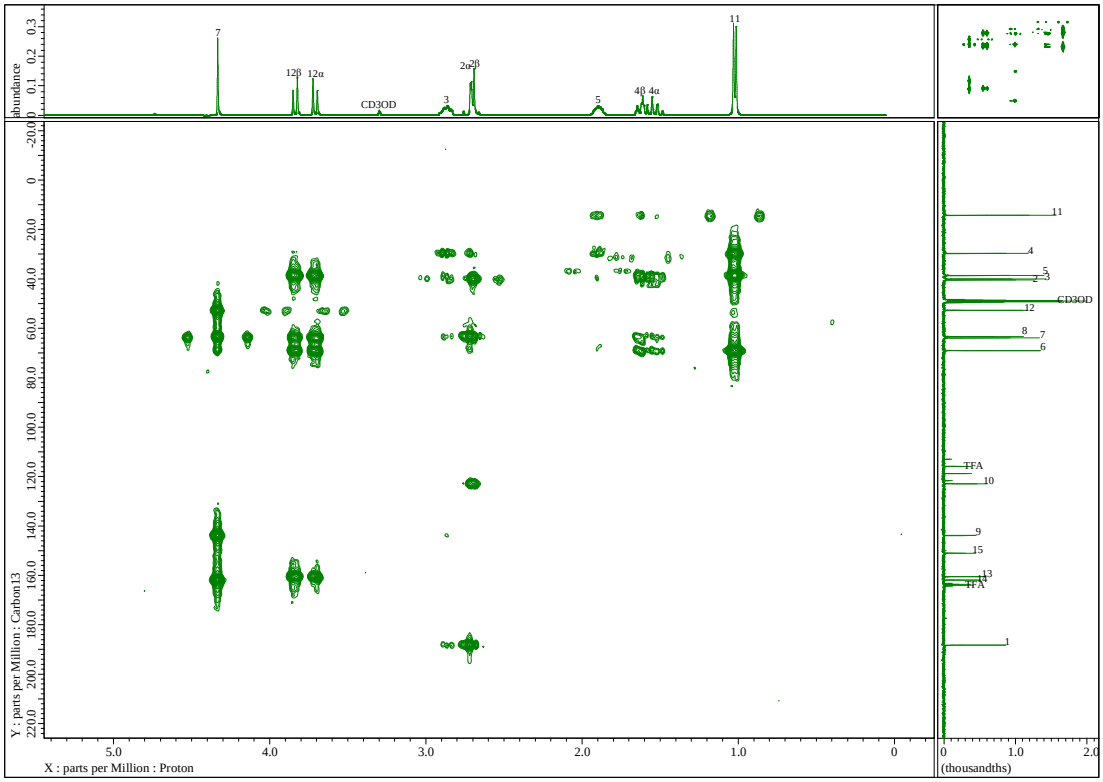

Figure S18. HMBC spectrum of **1** in D_2O with CD_3OD (400MHz).

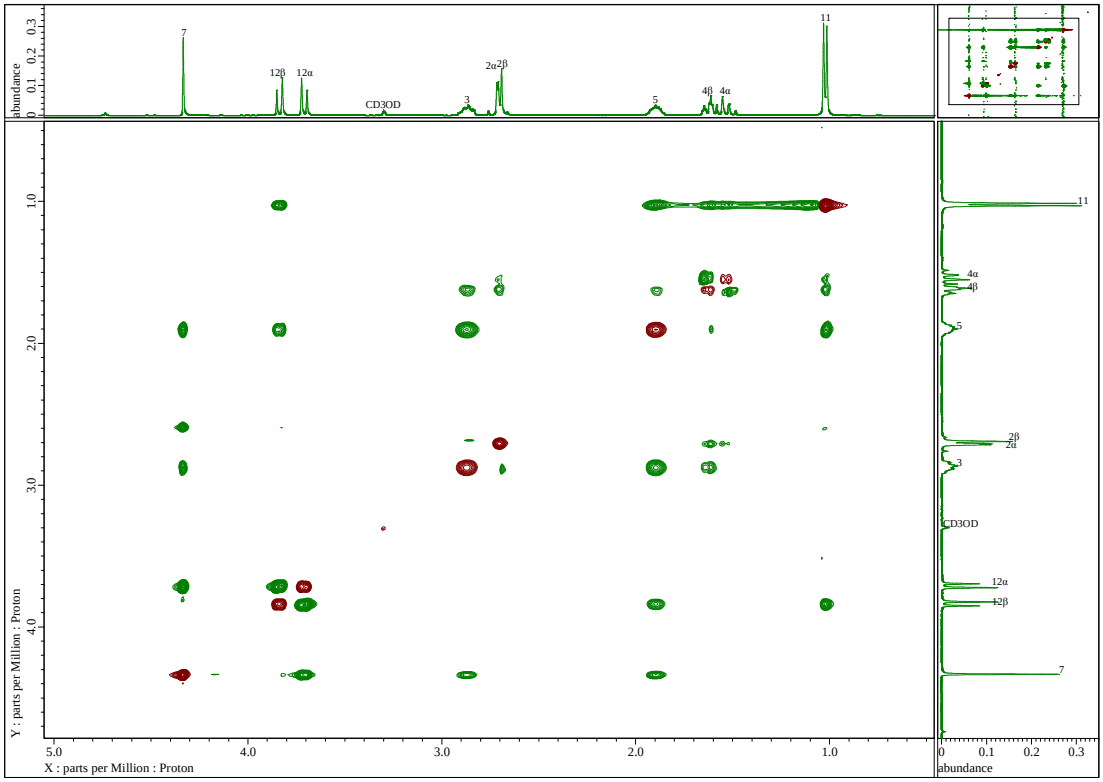

Figure S19. NOESY spectrum of **1** in D_2O with CD_3OD (400MHz).

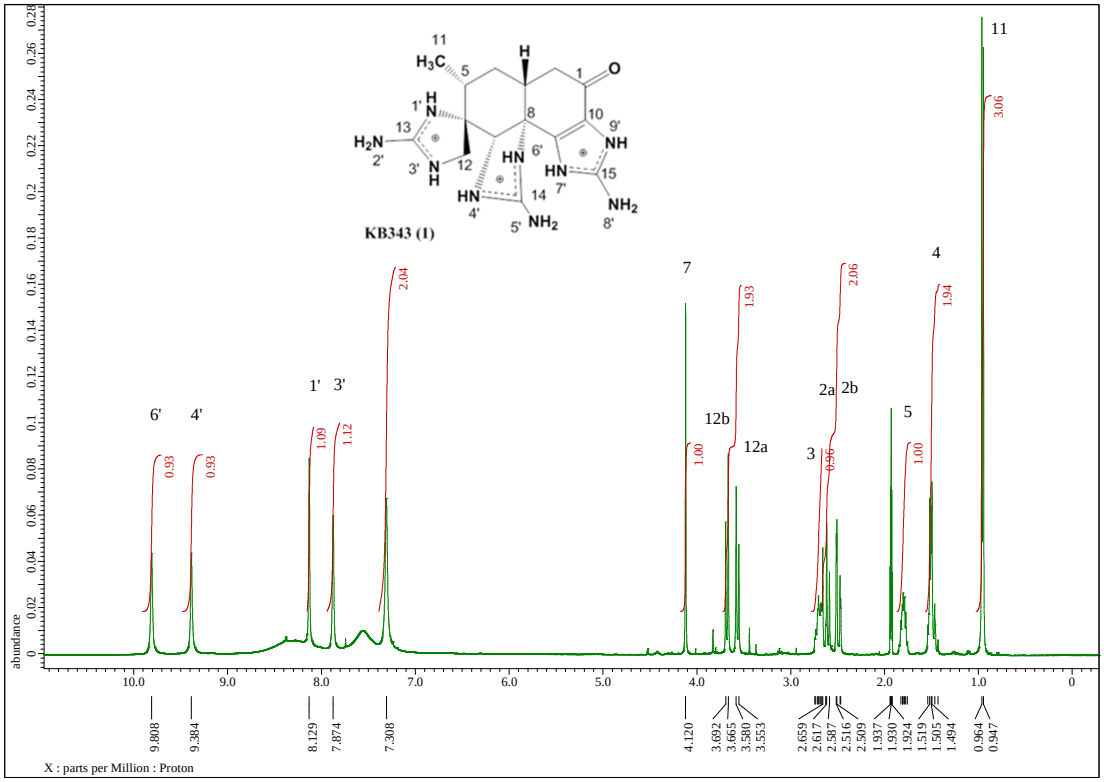

Figure S20. ^{1}H NMR spectrum of **1** in acetonitrile-d_3.

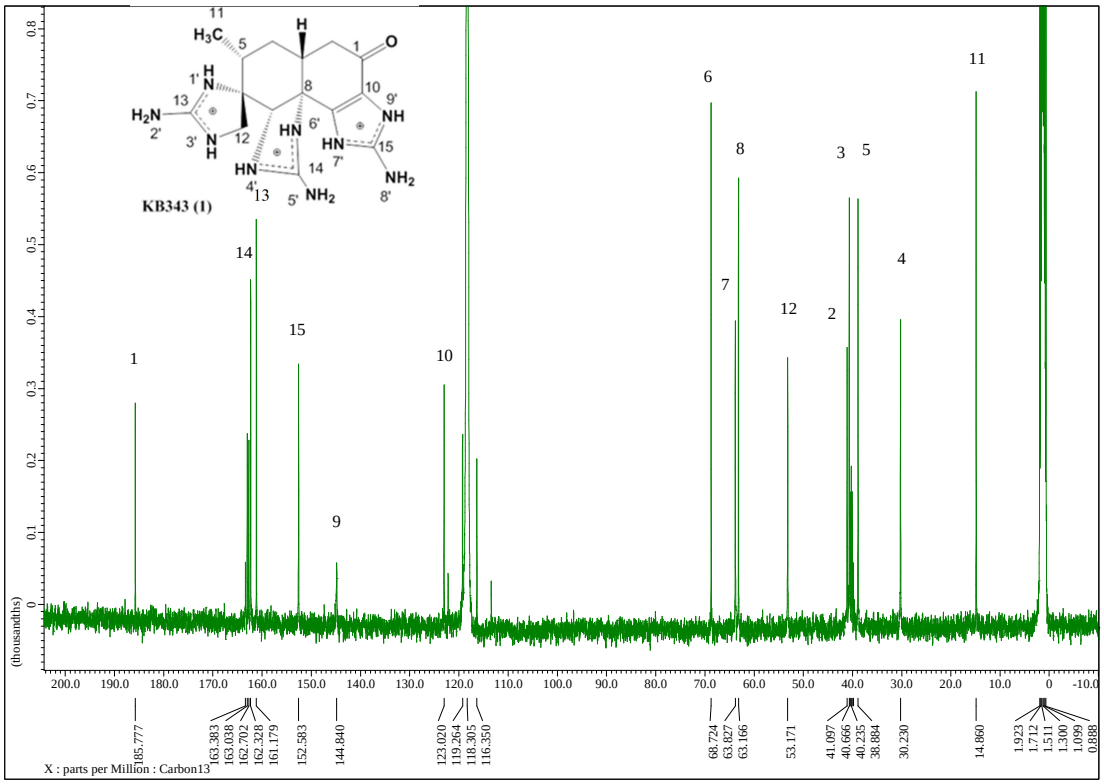

Figure S21. ^{13}C NMR spectrum of **1** (TFA salt) in acetonitrile-d_3.

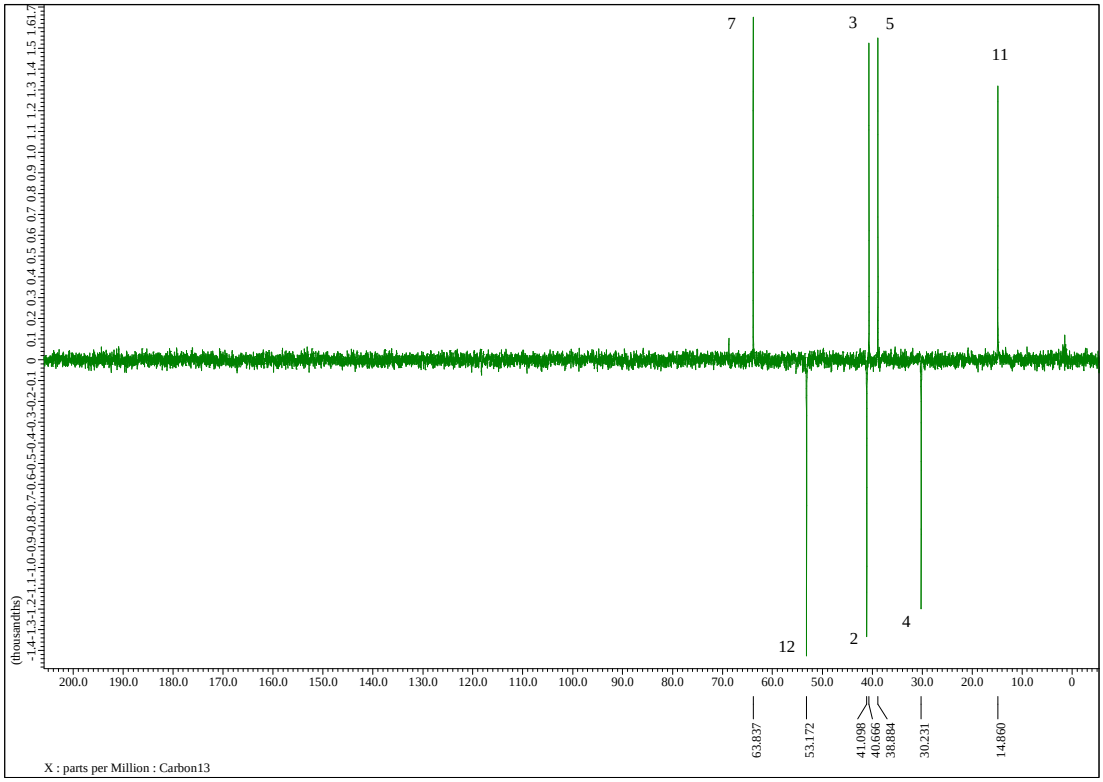

Figure S22. ^{13}C DEPT 135 spectrum of **1** in acetonitrile-d_3.

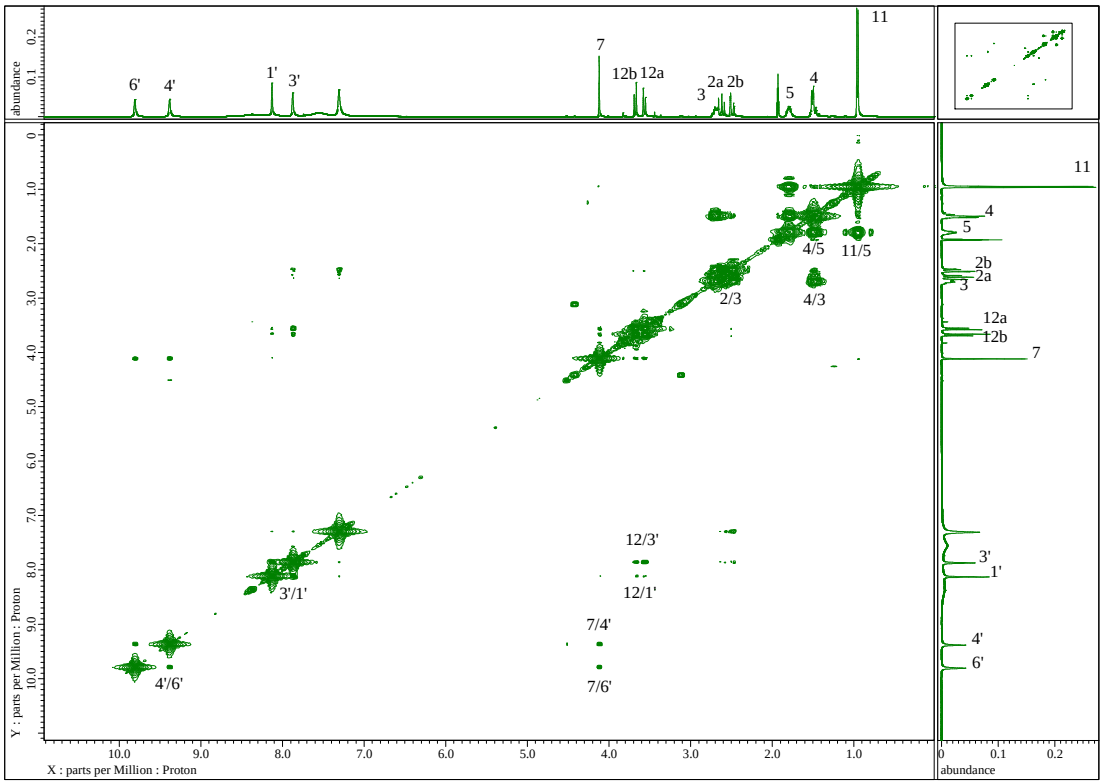

Figure S23. ^{1}H-^{1}H COSY spectrum of **1** in acetonitrile-d_3.

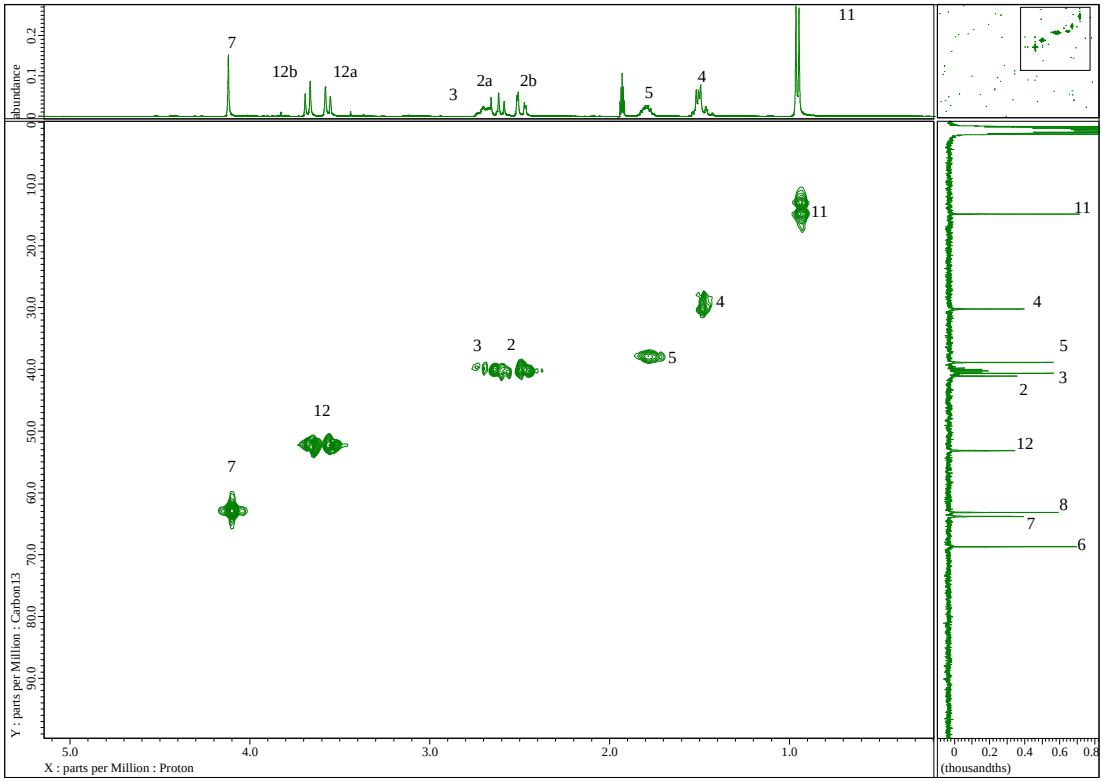

Figure S24. HMQC spectrum of **1** in acetonitrile-d_3.

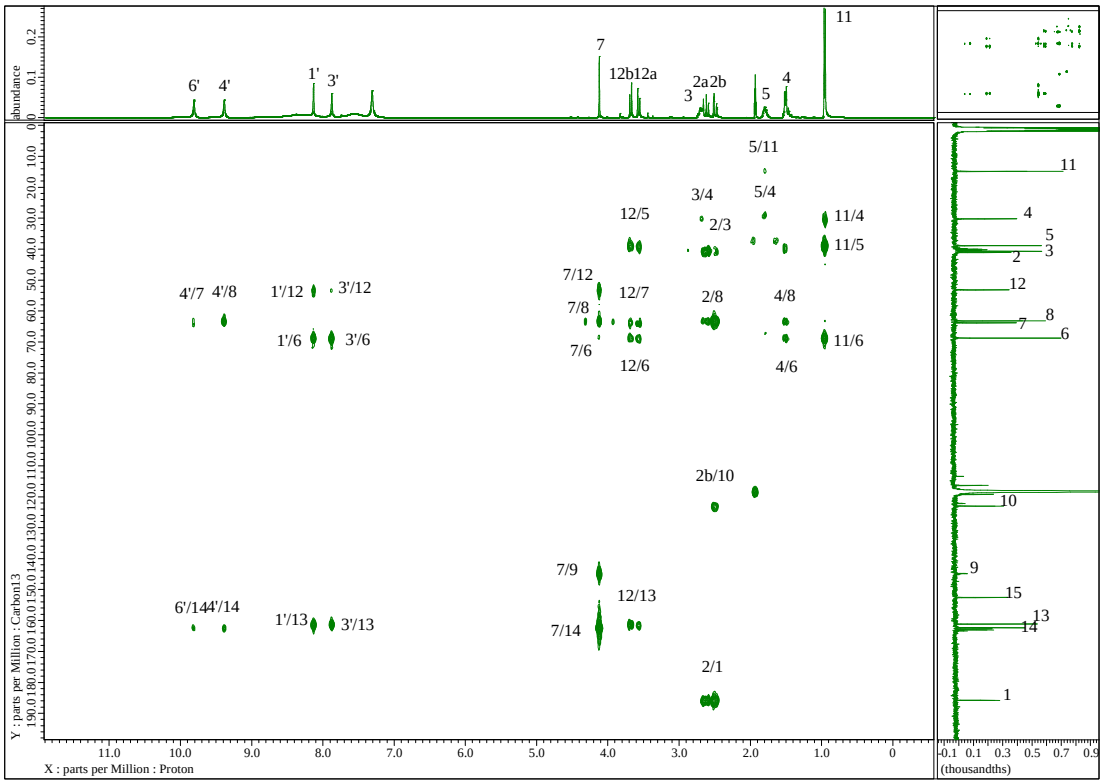

Figure S25. HMBC spectrum of **1** in CD_3CN-d_3. Long range is 8 Hz.

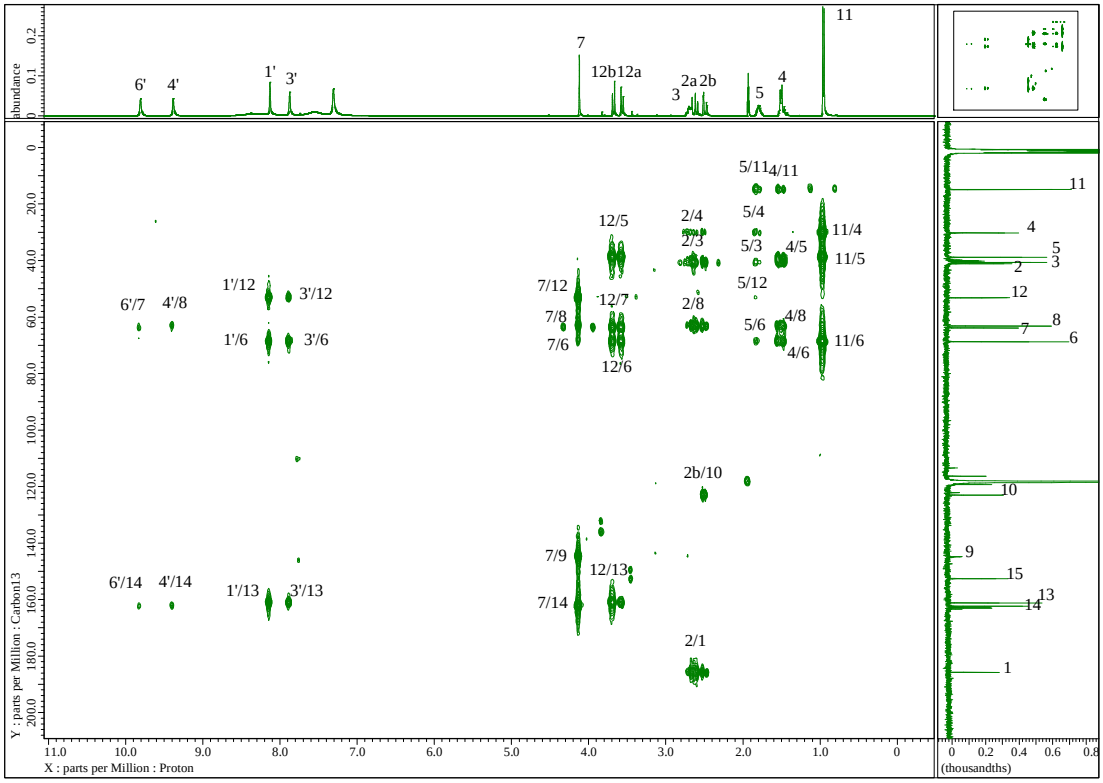

Figure S26. HMBC spectrum of **1** in CD_3CN-d_3.

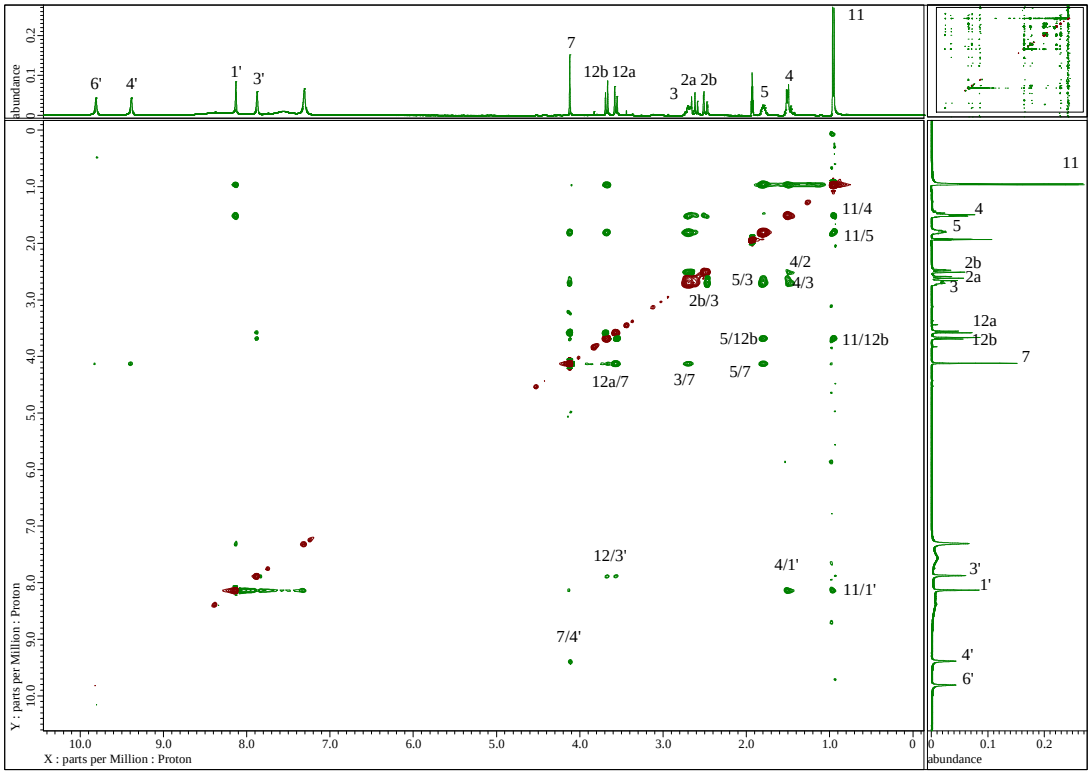

Figure S27. NOESY spectrum of **1** in acetonitrile-d_3.

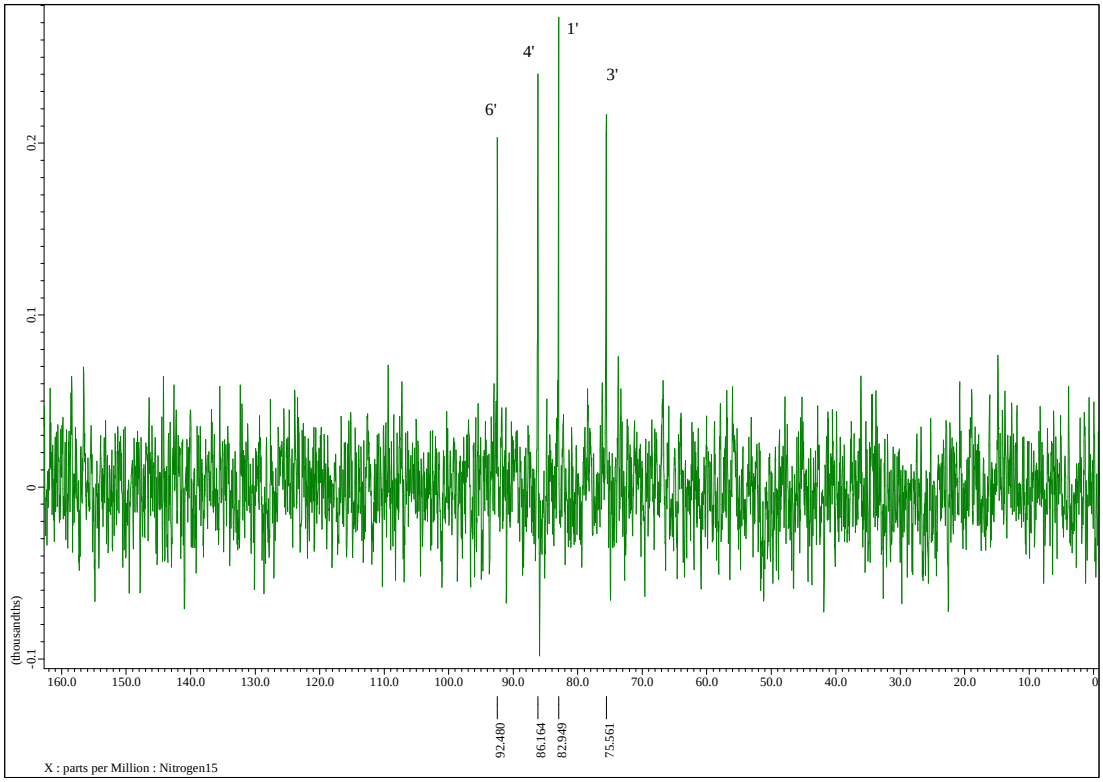

Figure S28. ^{15}N DEPT 135 spectrum of **1** in acetonitrile-d_3.

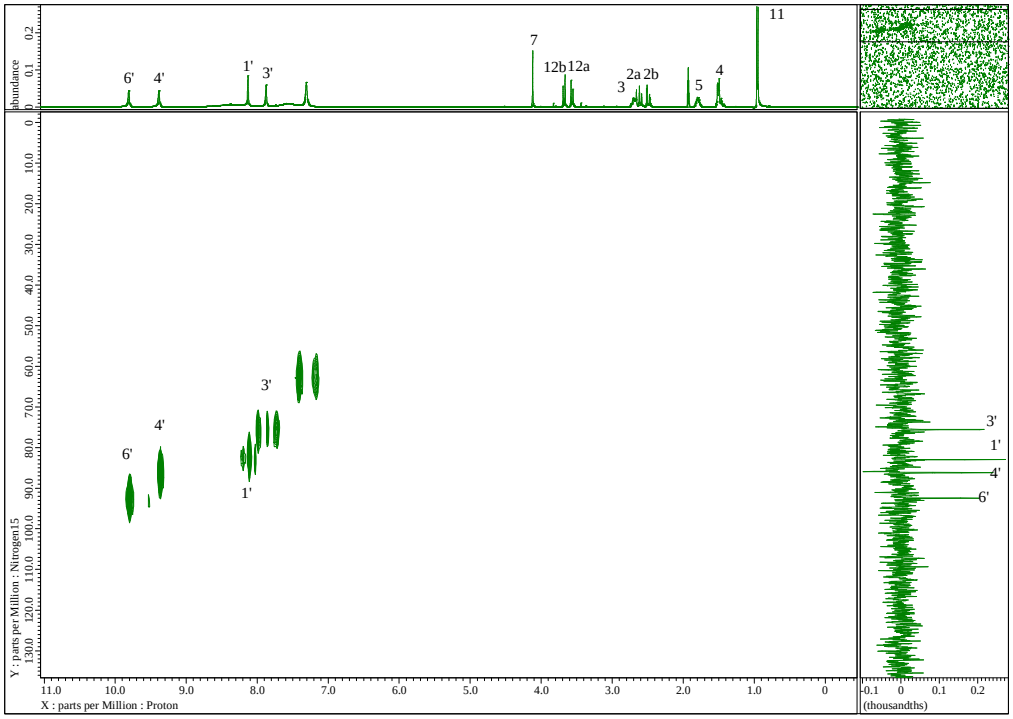

Figure S29. ^{15}N HSQC spectrum of **1** in acetonitrile-d_3.

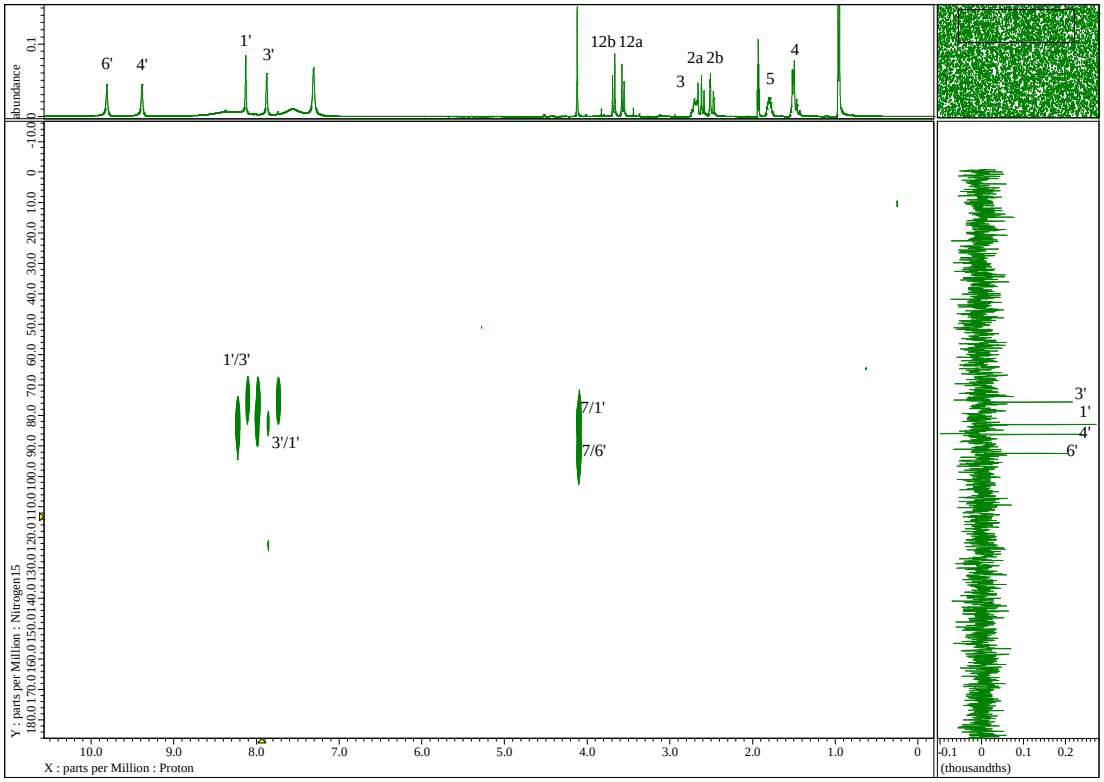

Figure S30. ^{15}N HMBC spectrum of **1** in acetonitrile-d_3.

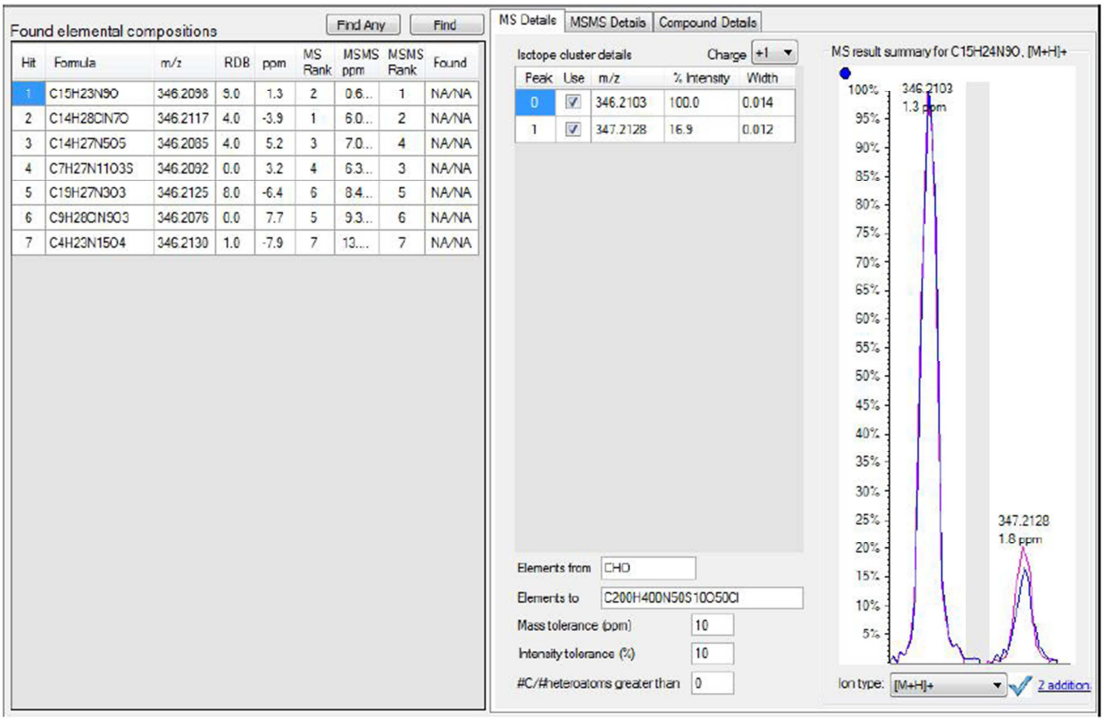

Figure S31. Q-TOF High resolution LC/MS data of **5**.

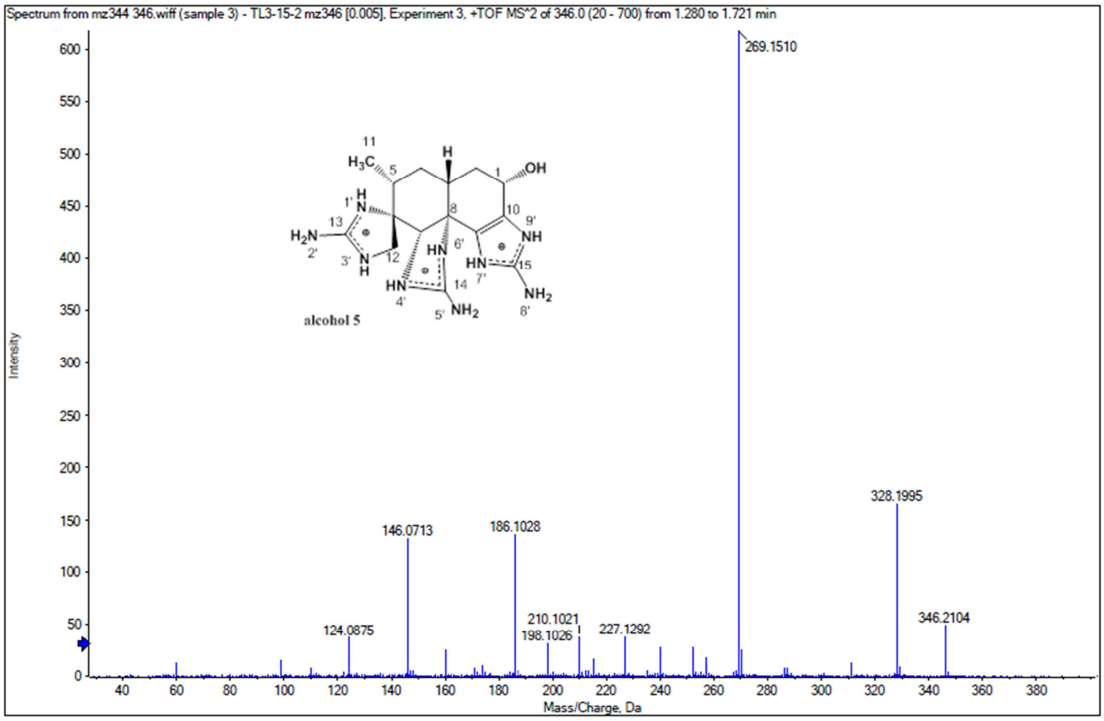

Figure S32. Q-TOF High resolution LC/MS/MS data of **5**. Collision Energy (CE) 30 V.

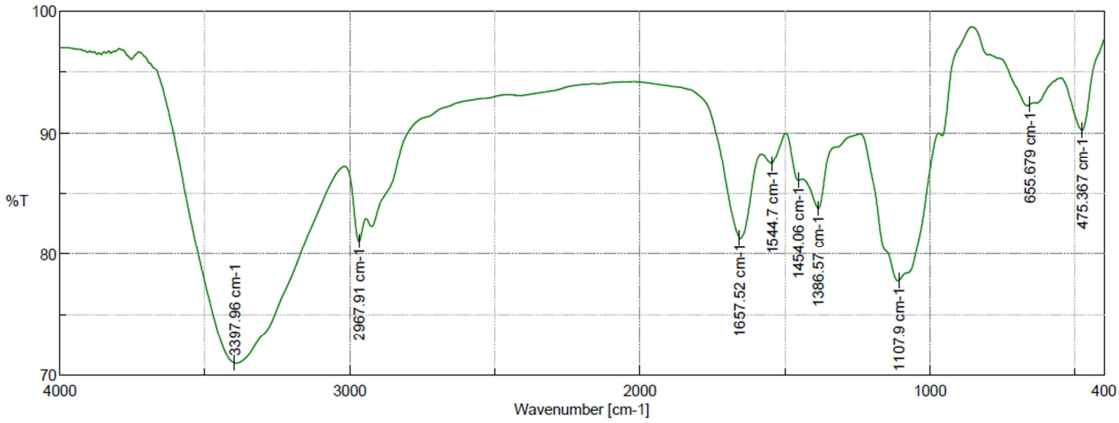

Figure S33. IR spectrum (KBr) of **5**.

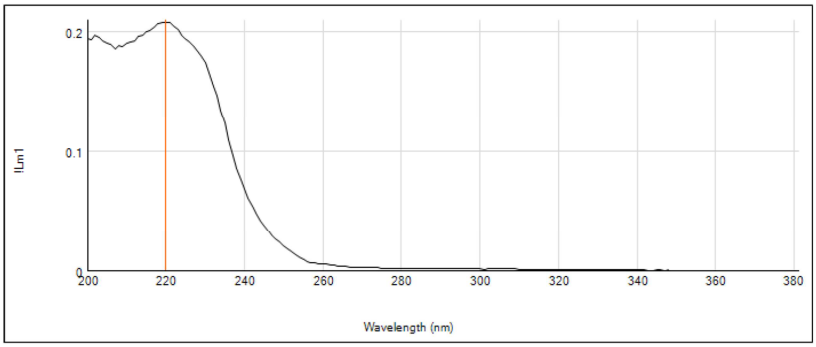

Figure S34. UV spectrum (H_2O) of **5**.

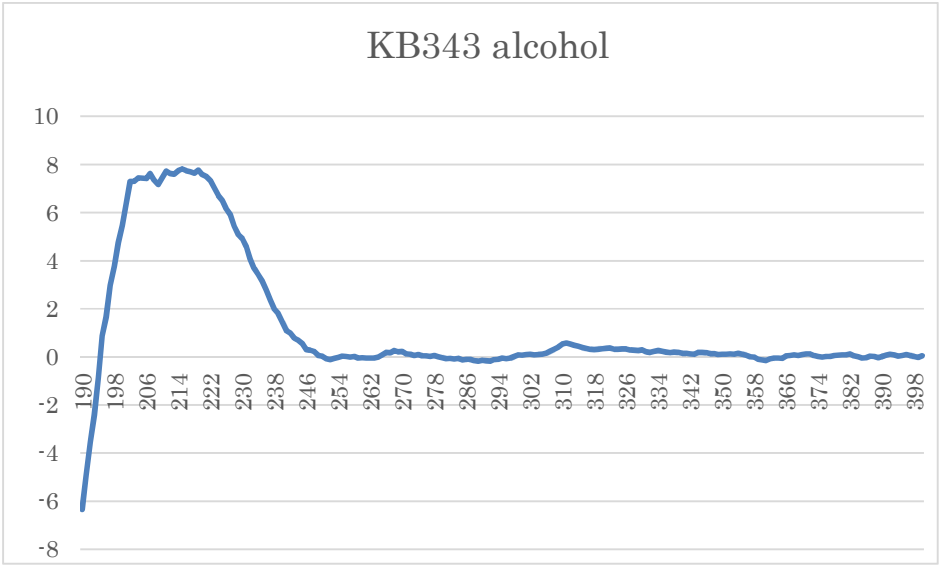

Figure S35. CD spectrum (H_2O) of **5**.

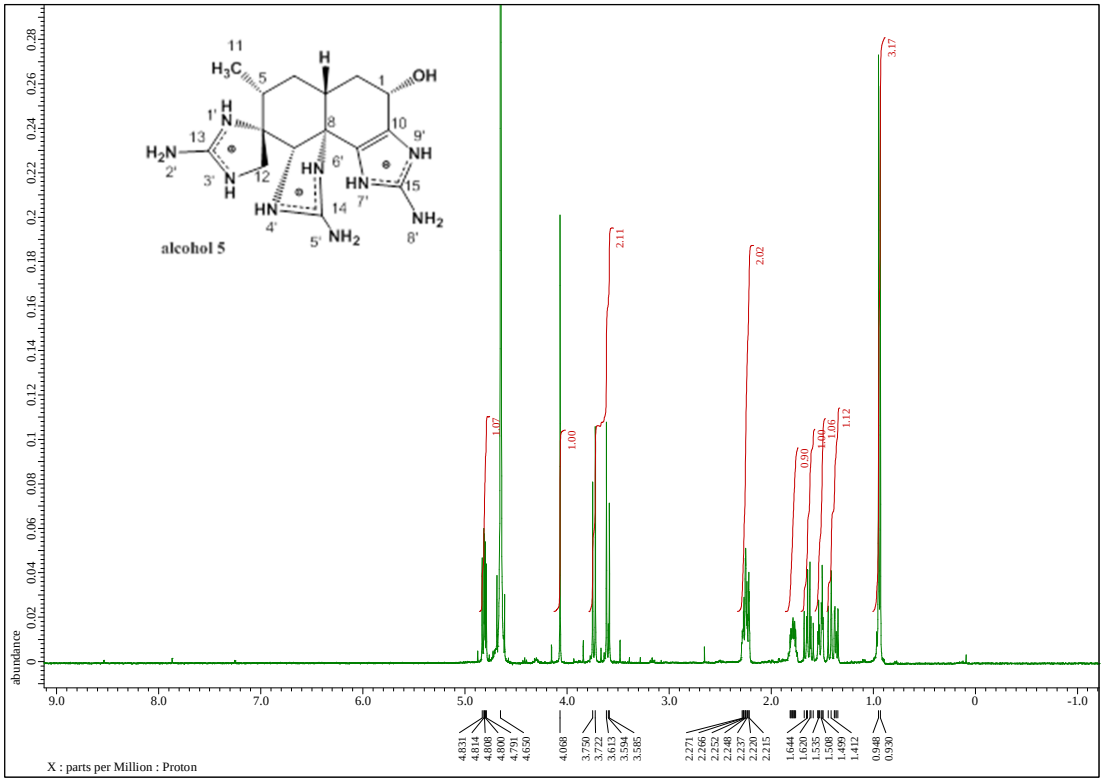

Figure S36. ^{1}H NMR spectrum of **5** in D_2O (400 MHz).

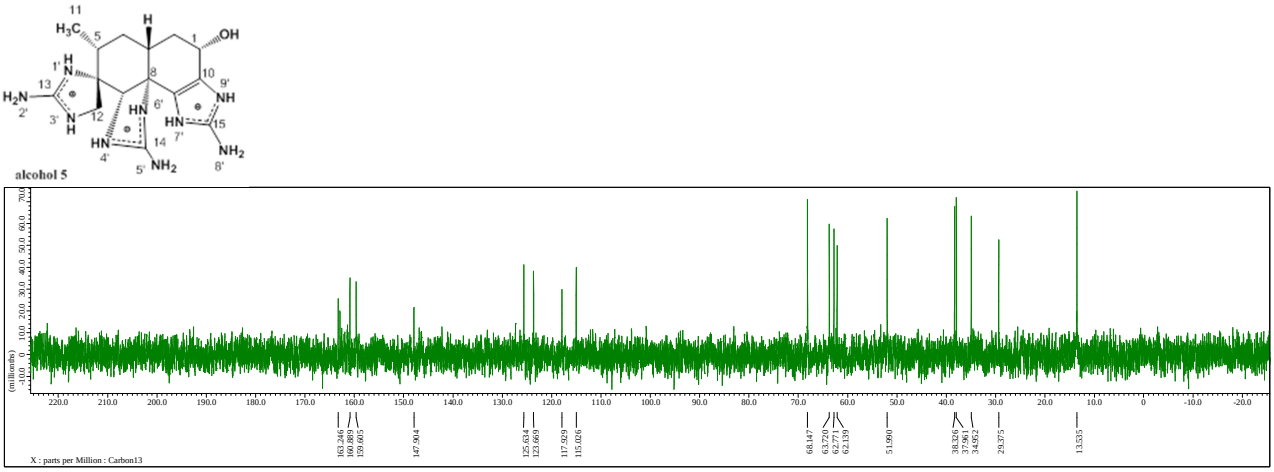

Figure S37. ^{13}C NMR spectrum of **5** (TFA salt) in D_2O (100 MHz).

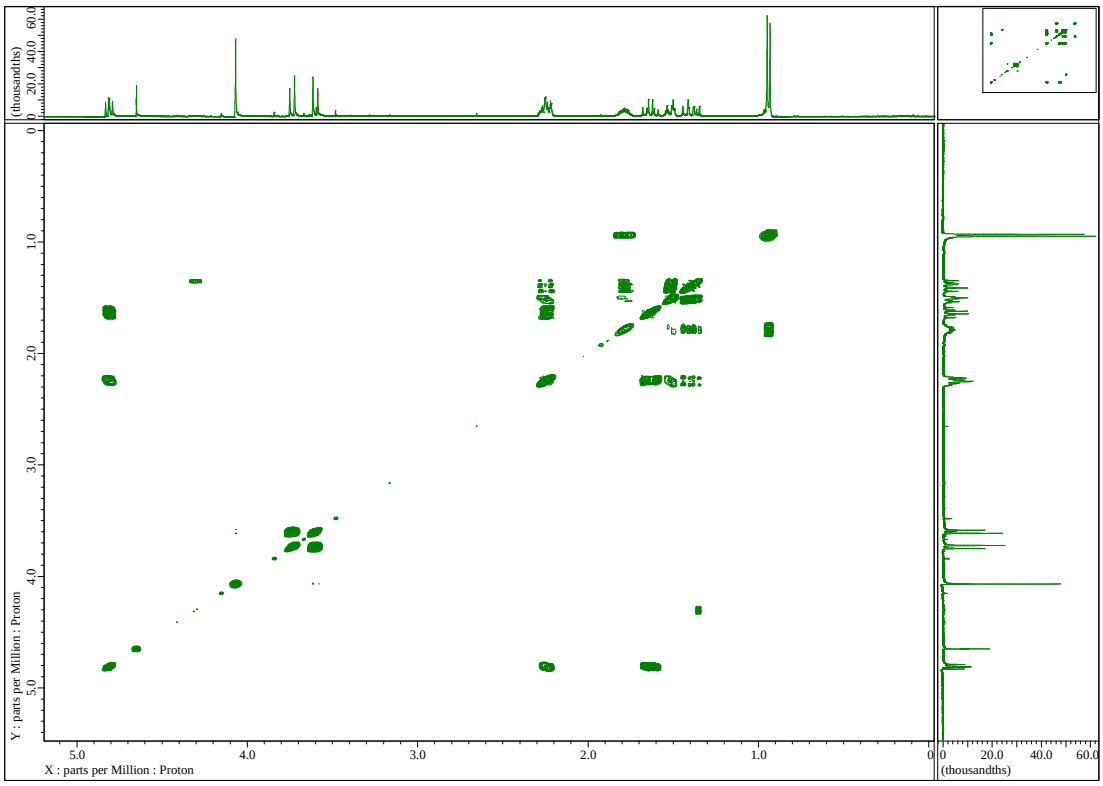

Figure S38. ^{1}H-^{1}H COSY spectrum of **5** in D_2O (400 MHz).

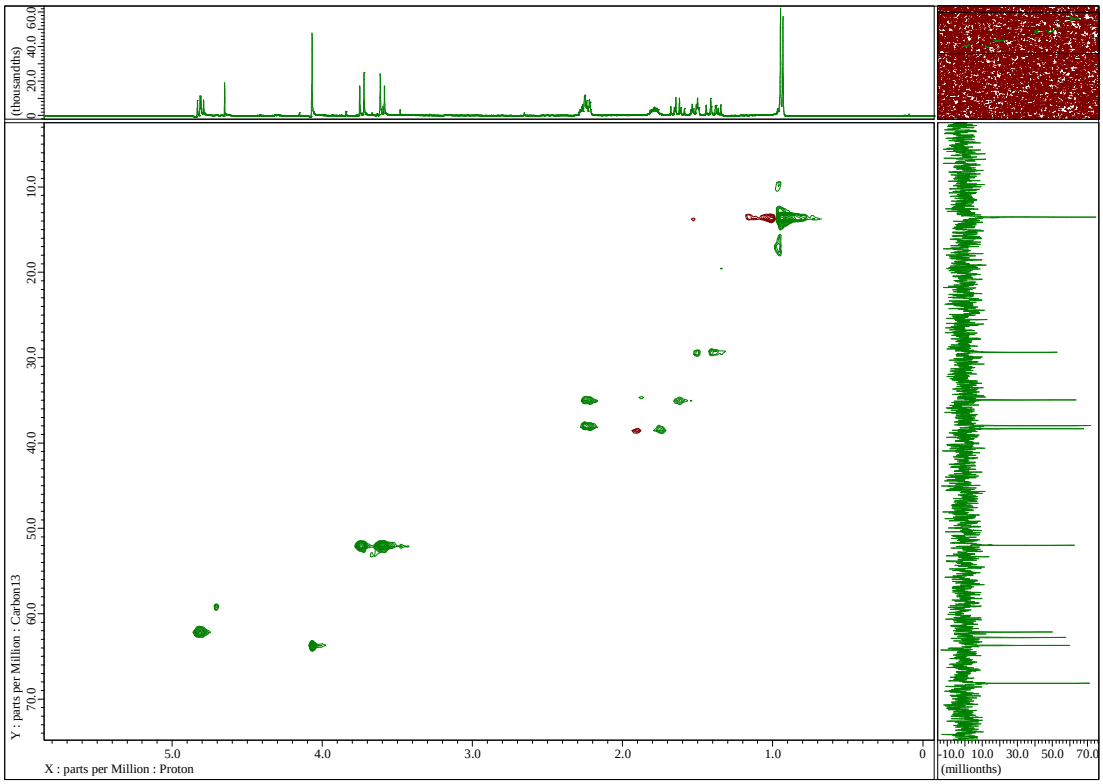

Figure S39. HSQC spectrum of **5** in D_2O (400 MHz).

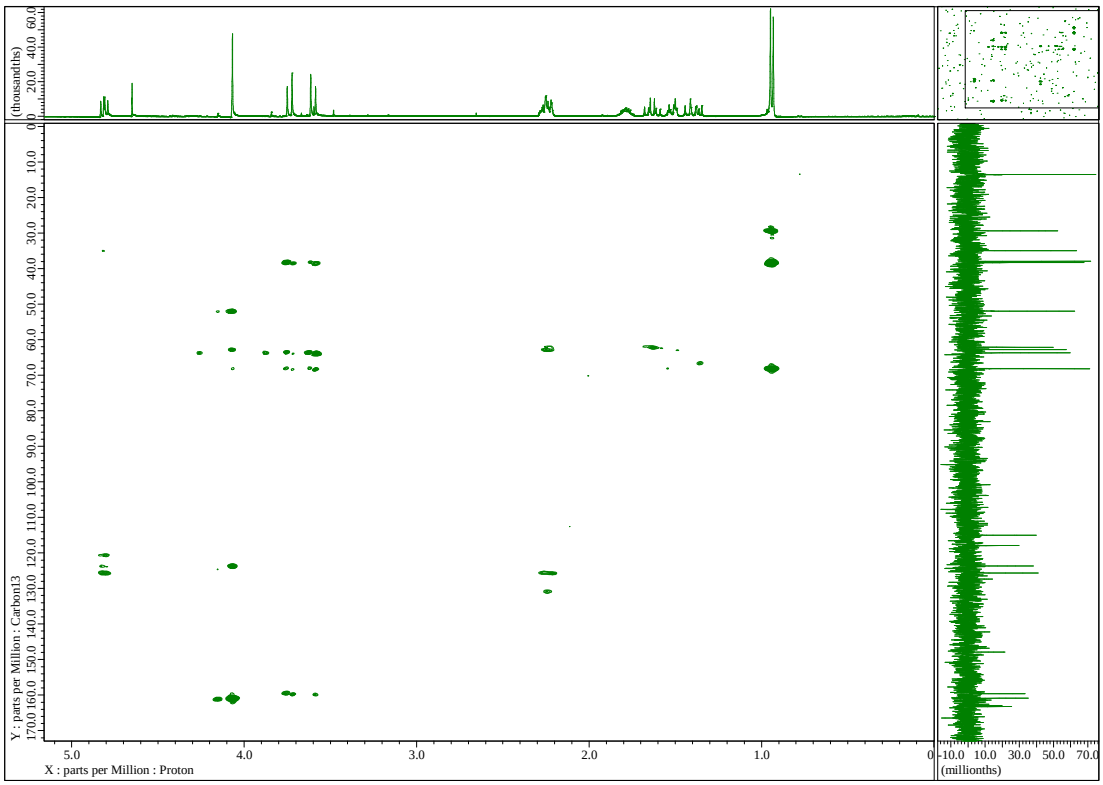

Figure S40. HMBC spectrum of **5** in D_2O (400 MHz).

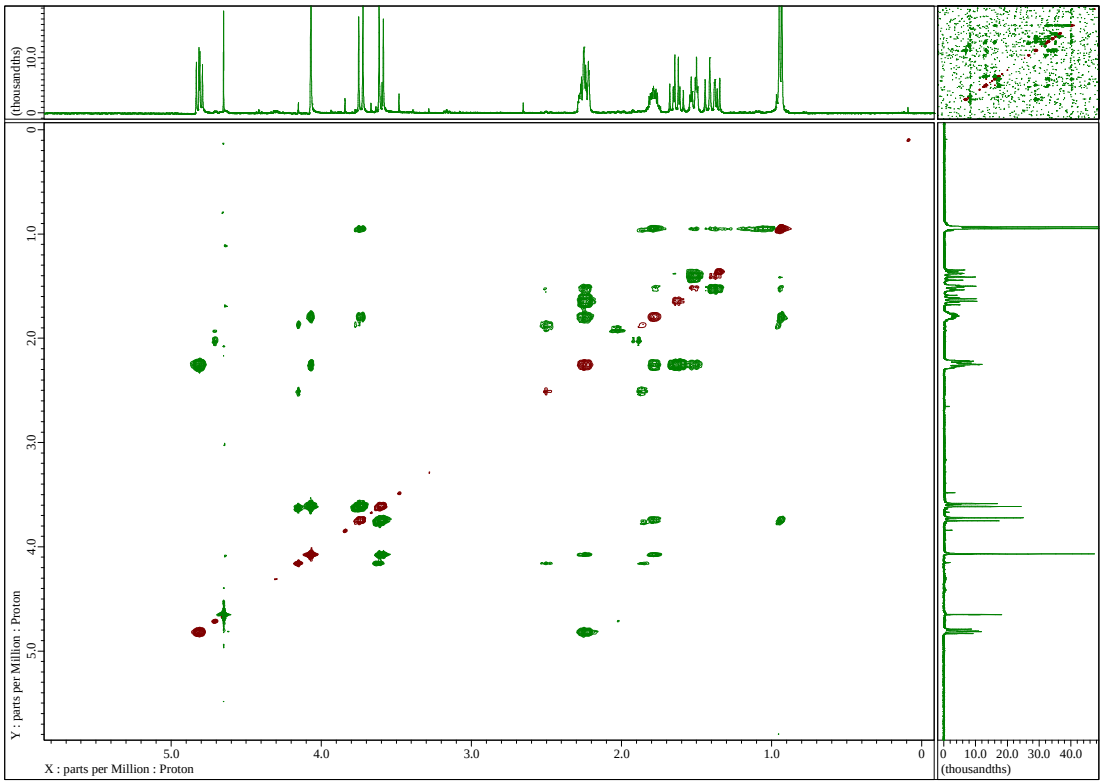

Figure S41. NOESY spectrum of **5** in D_2O (400 MHz).

(A) (B)

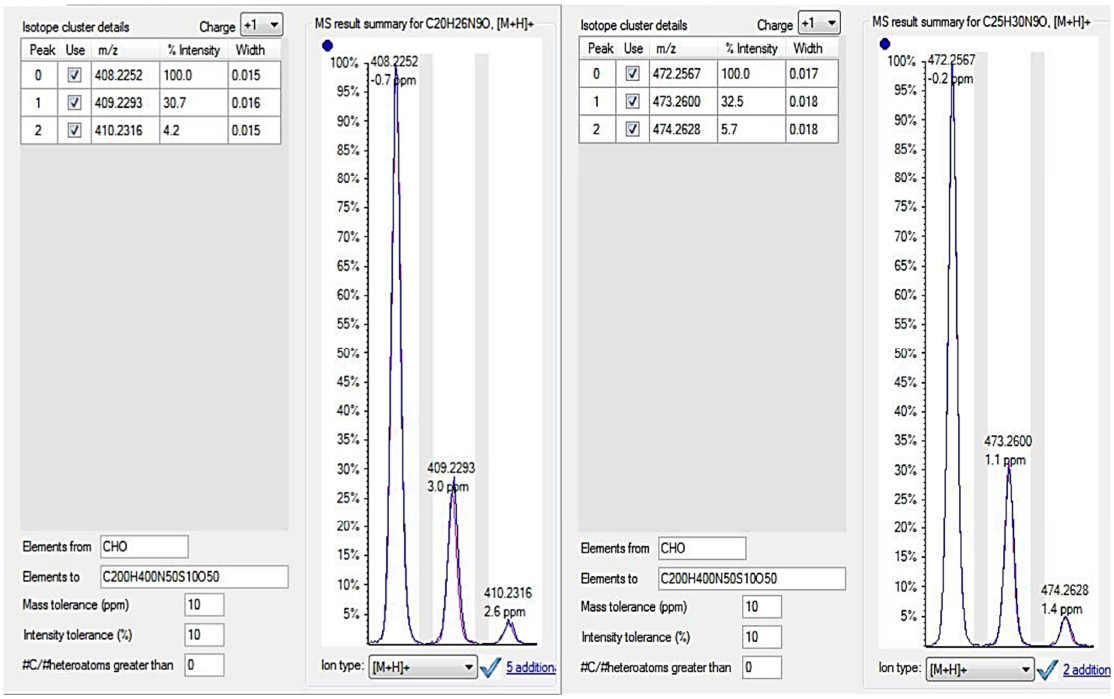

(C)

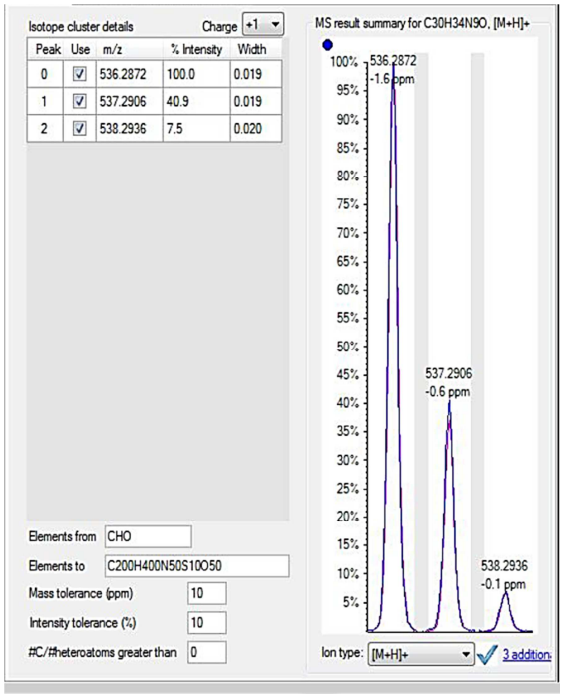

Figure S42**.** Q-TOF High resolution ESIMS data of pyrimidine derivatives of **1**.

(A) Monopyrimidine derivative (**2**). (B) Bispyrimidine derivative (**3**). (C) Trispyrimidine derivative (**4**).

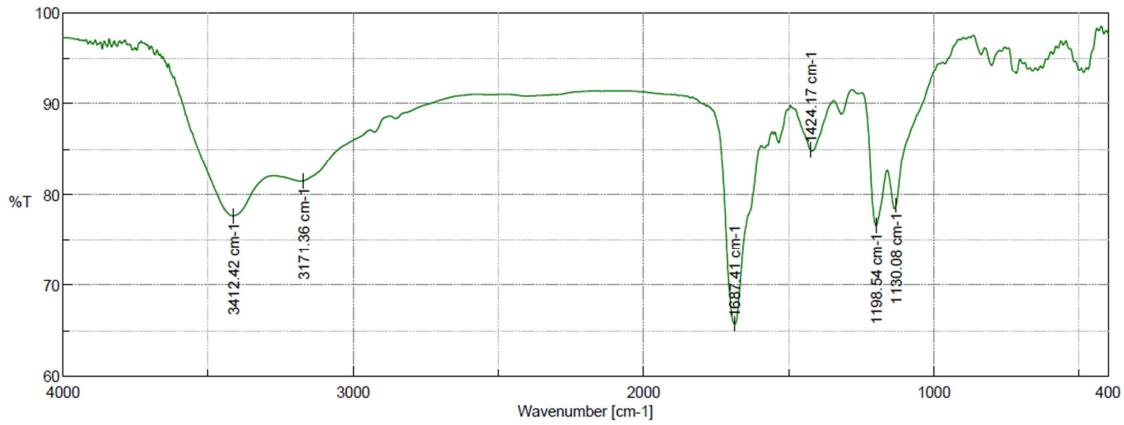

Figure S43. IR spectrum (KBr) of **2**.

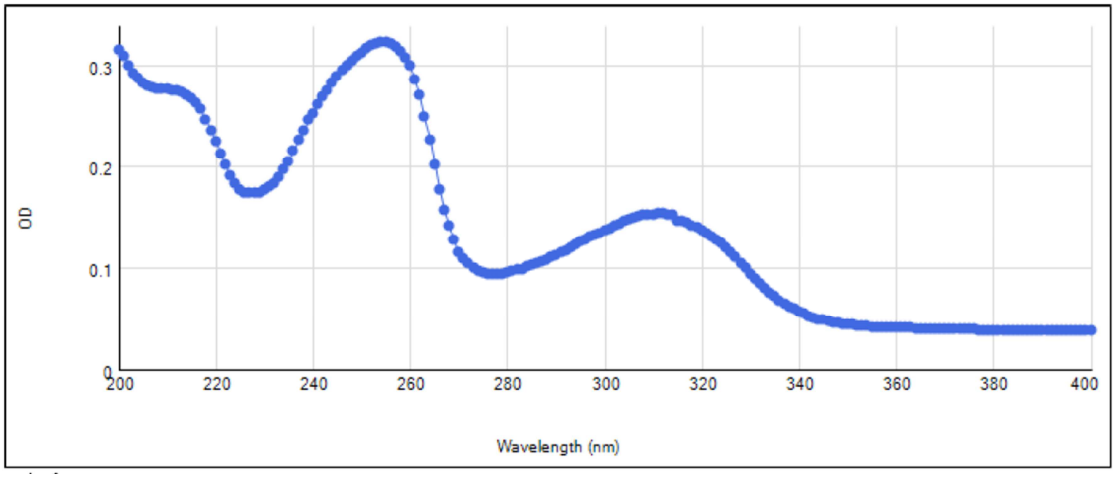

Figure S44. UV spectrum (H_2O) of **2**.

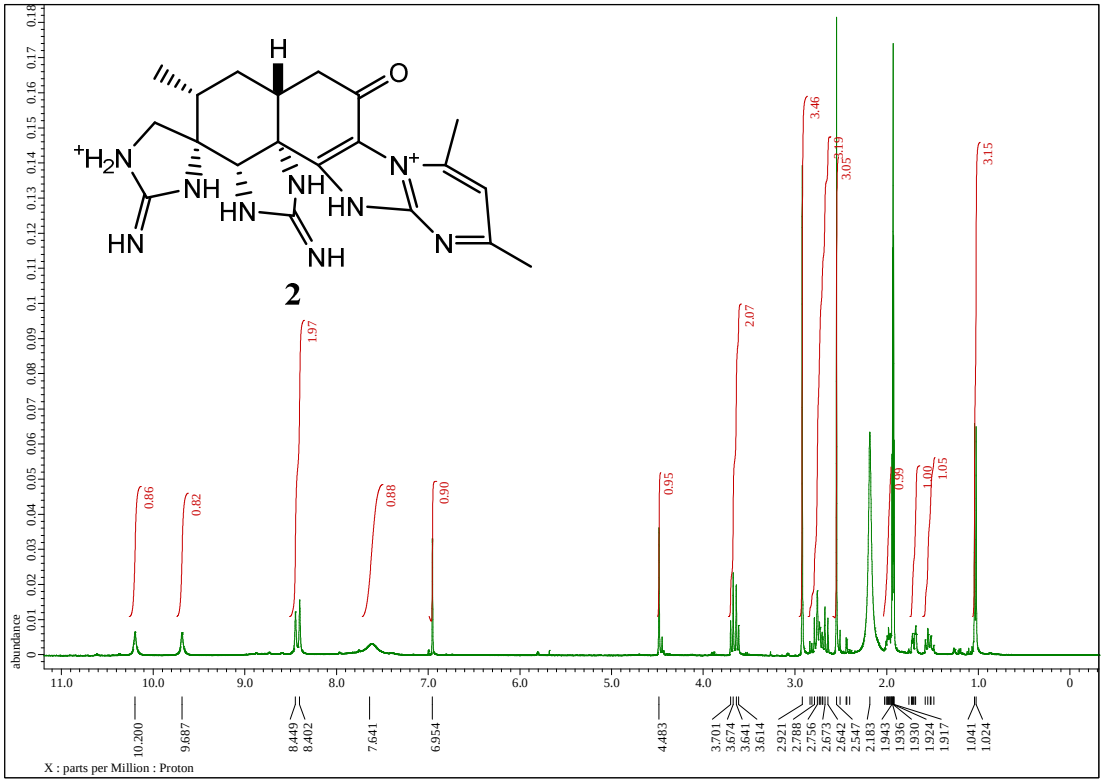

Figure S45. ^{1}H NMR spectrum of compound **2** in CD_3CN-d_3 (400 MHz).

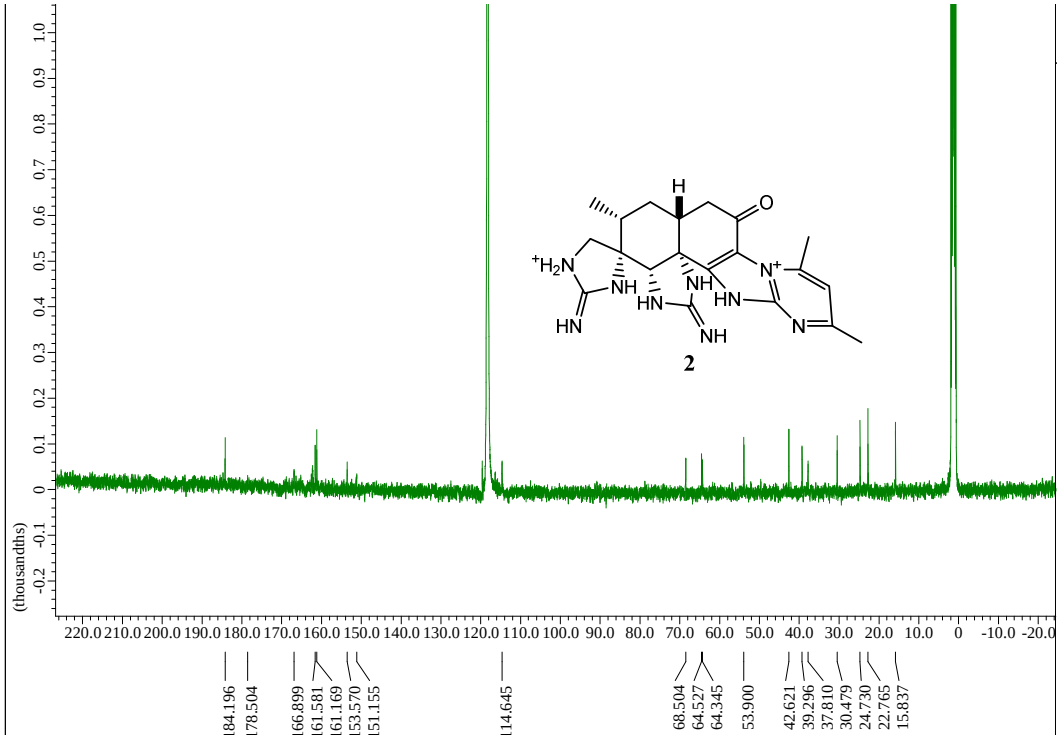

Figure S46. ^{13}C NMR spectrum of compound **2** in CD_3CN-d_3 (100 MHz).

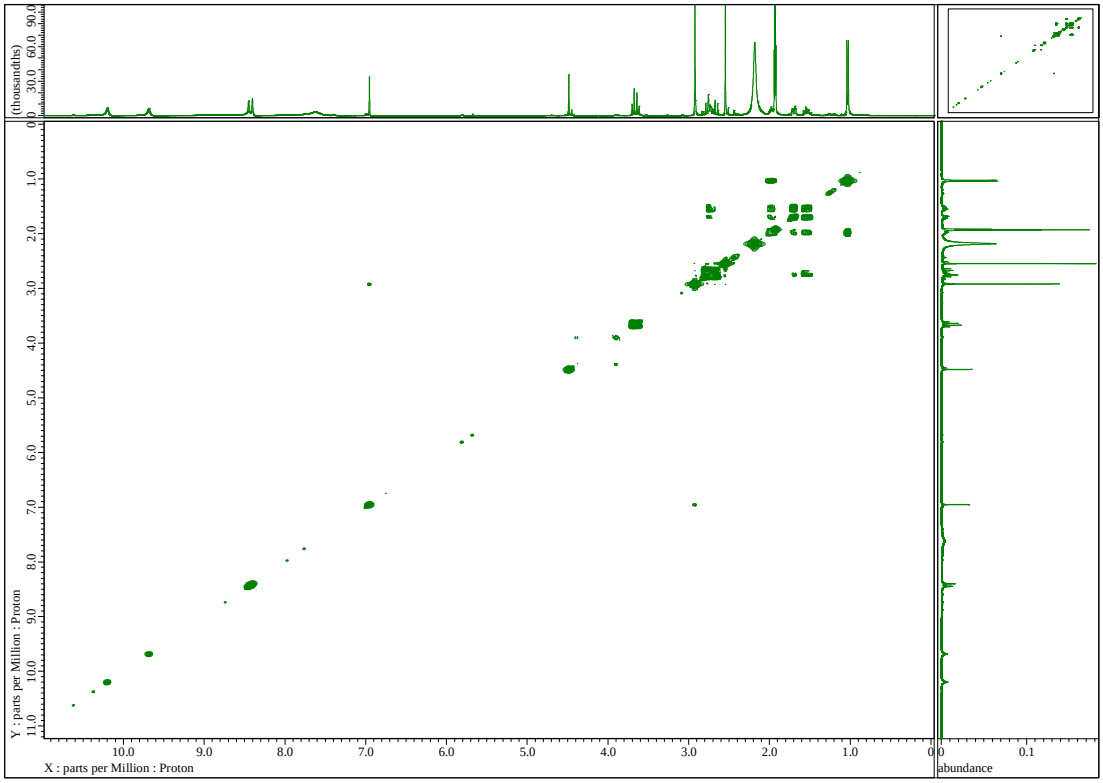

Figure S47. COSY spectrum of compound **2** in CD_3CN-d_3 (400 MHz).

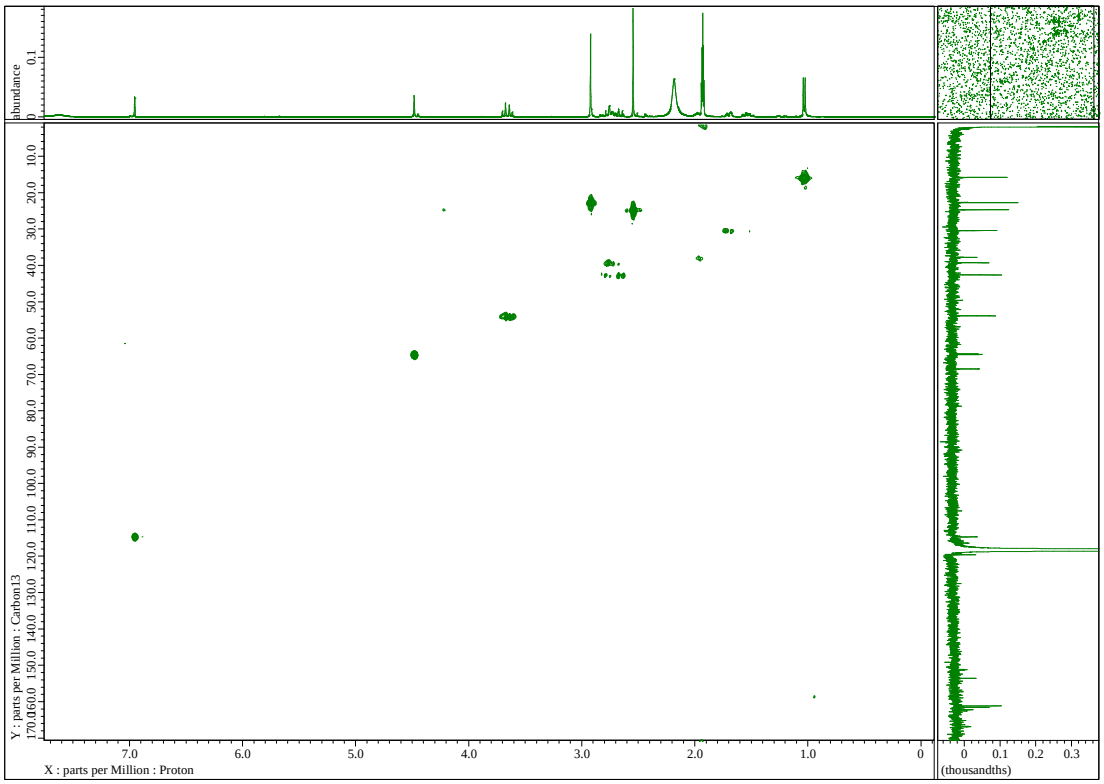

Figure S48. HMQC spectrum of compound **2** in CD_3CN-d_3 (400 MHz).

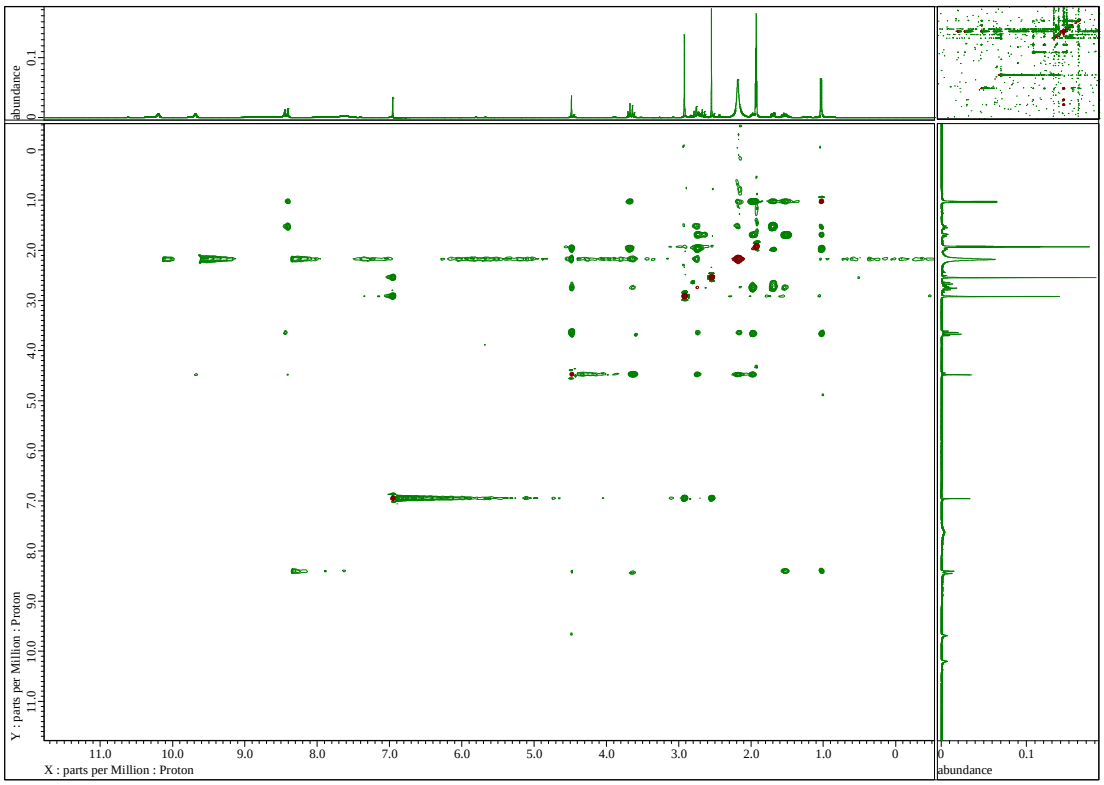

Figure S49. NOESY spectrum of compound **2** in CD_3CN-d_3 (400 MHz).

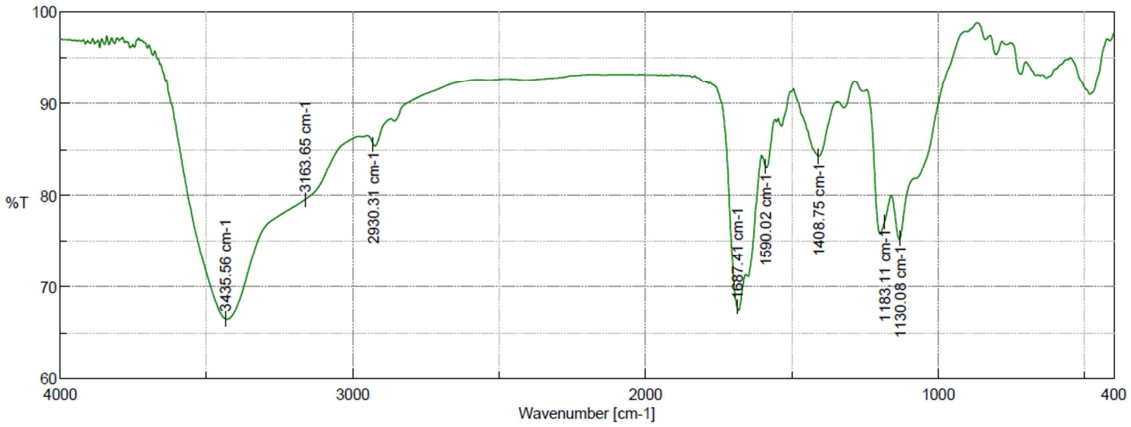

Figure S50. IR spectrum (KBr) of **3**.

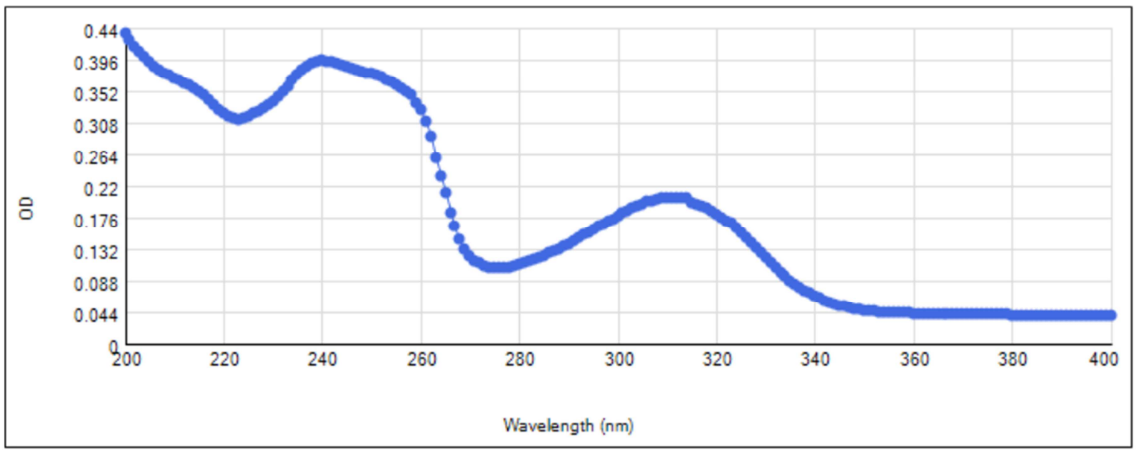

Figure S51. UV spectrum (H_2O) of **3**.

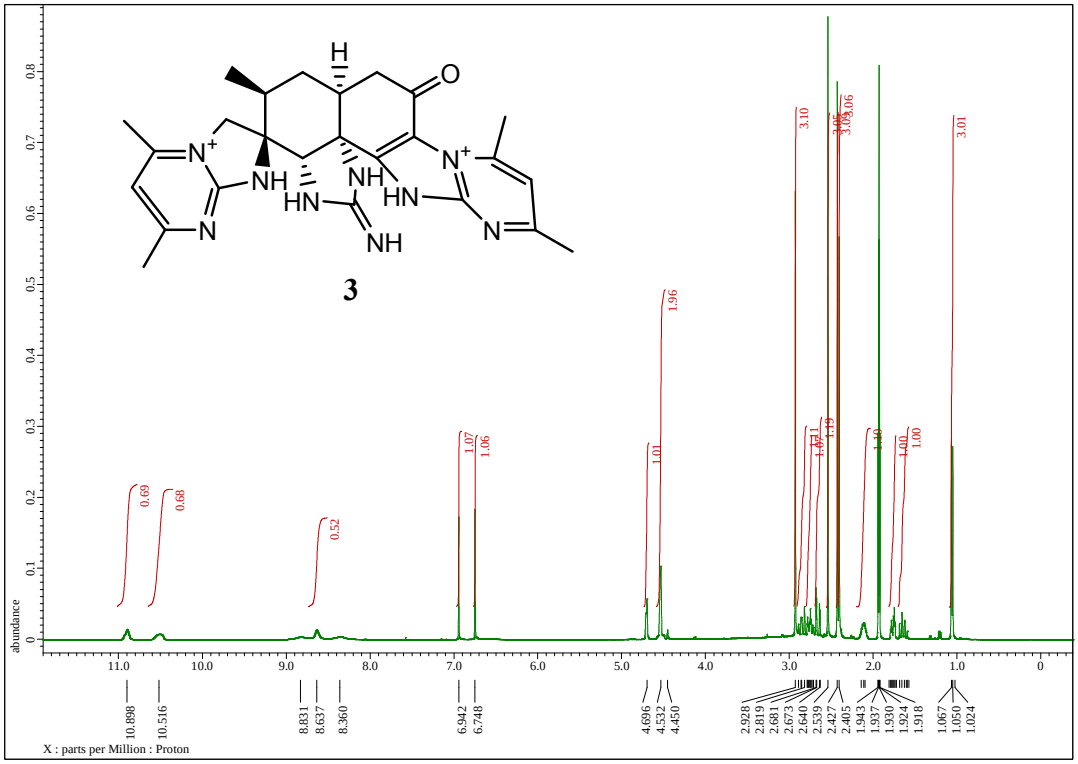

Figure S52. ^{1}H NMR spectrum of compound **3** in CD_3CN-d_3 (400 MHz).

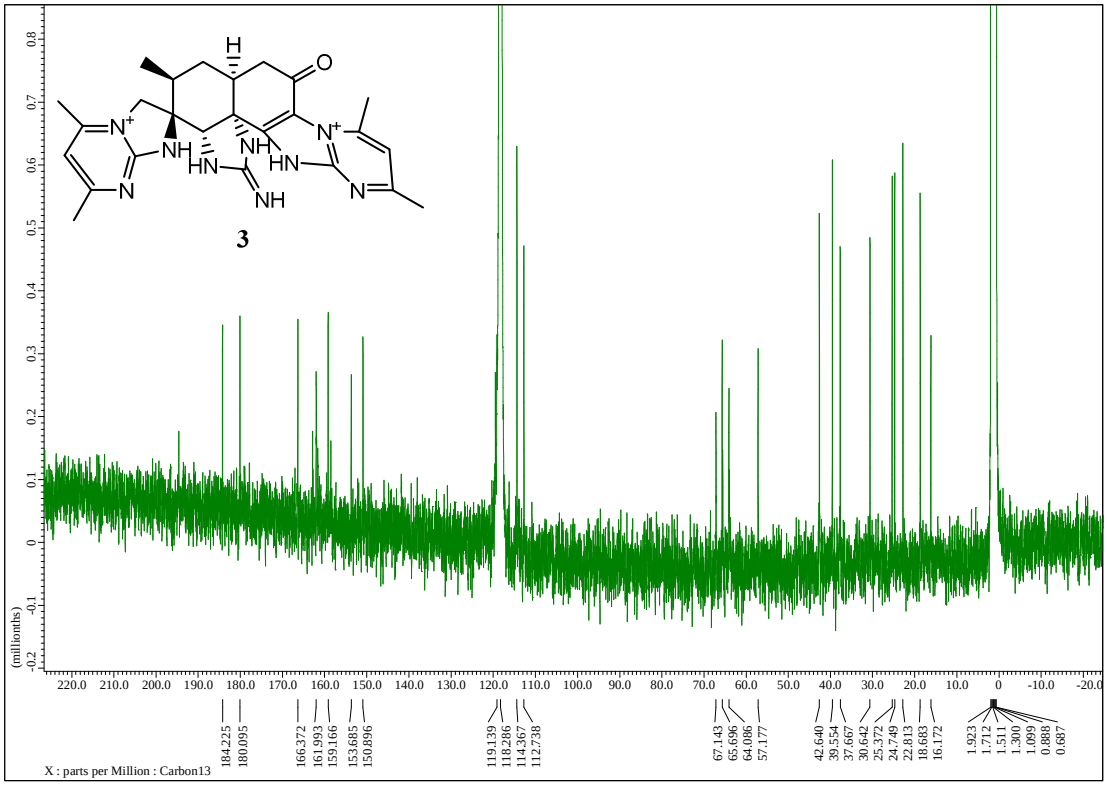

Figure S53. ^{13}C NMR spectrum of compound **3** in CD_3CN-d_3 (100 MHz).

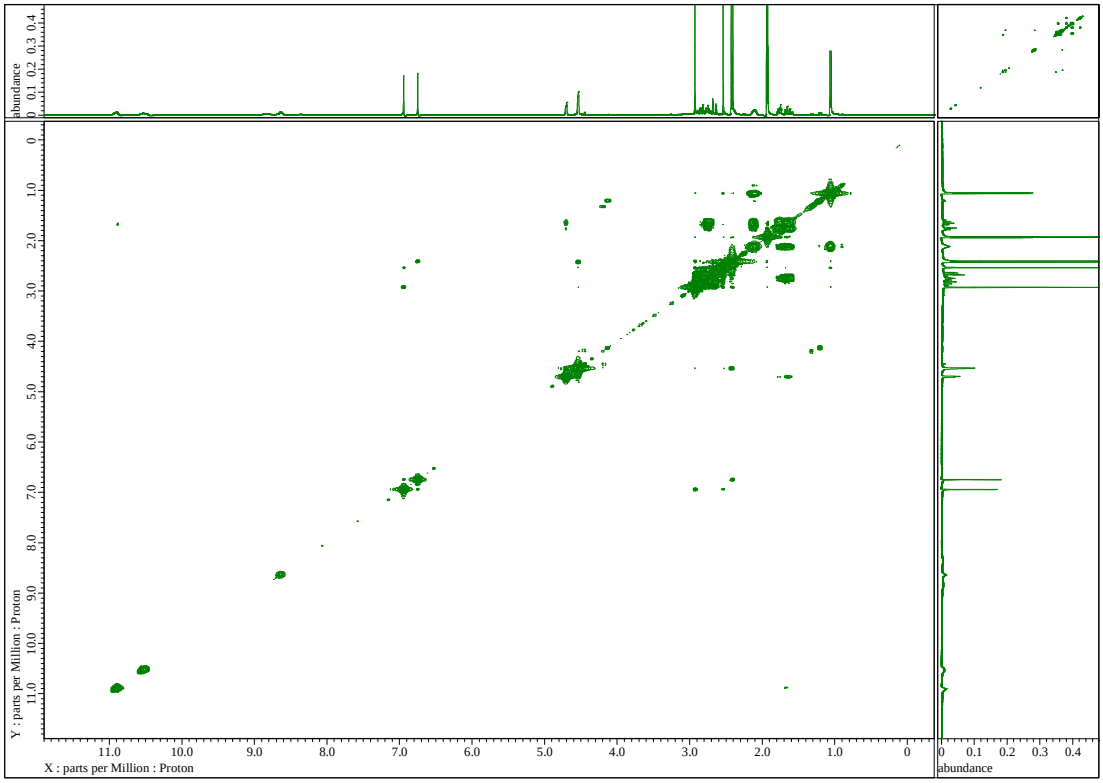

Figure S54. COSY spectrum of compound **3** in CD_3CN-d_3 (400 MHz).

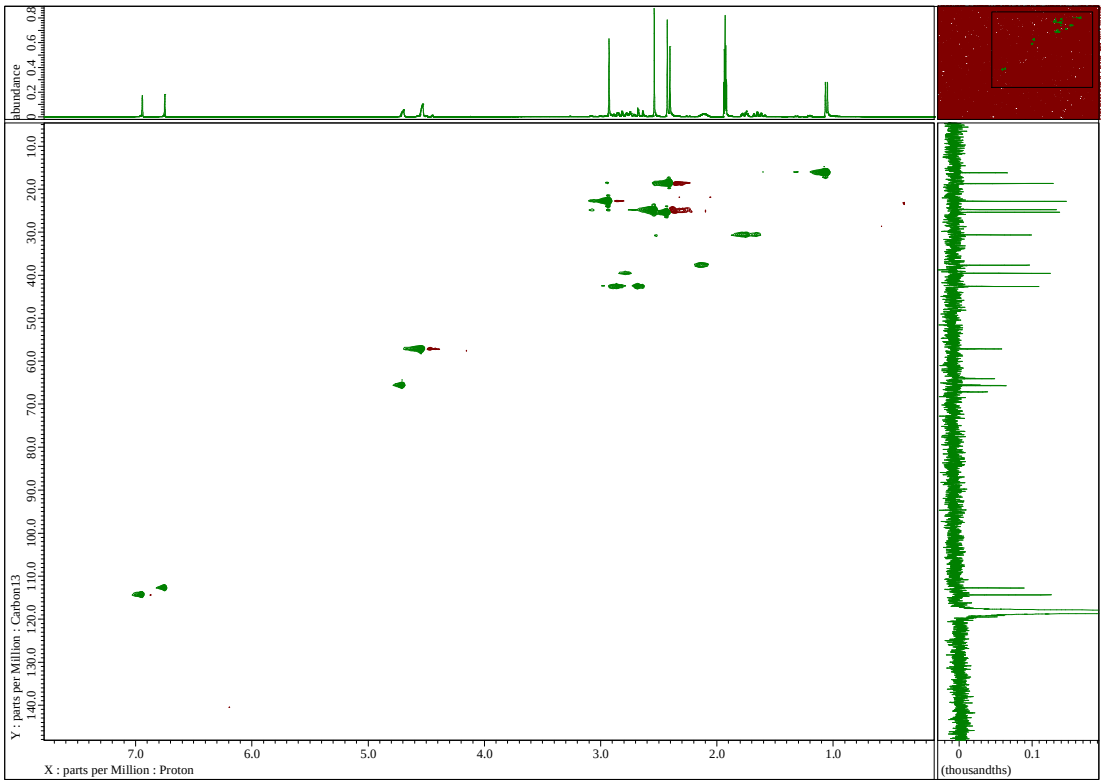

Figure S55. HSQC spectrum of compound **3** in CD_3CN-d_3 (400 MHz).

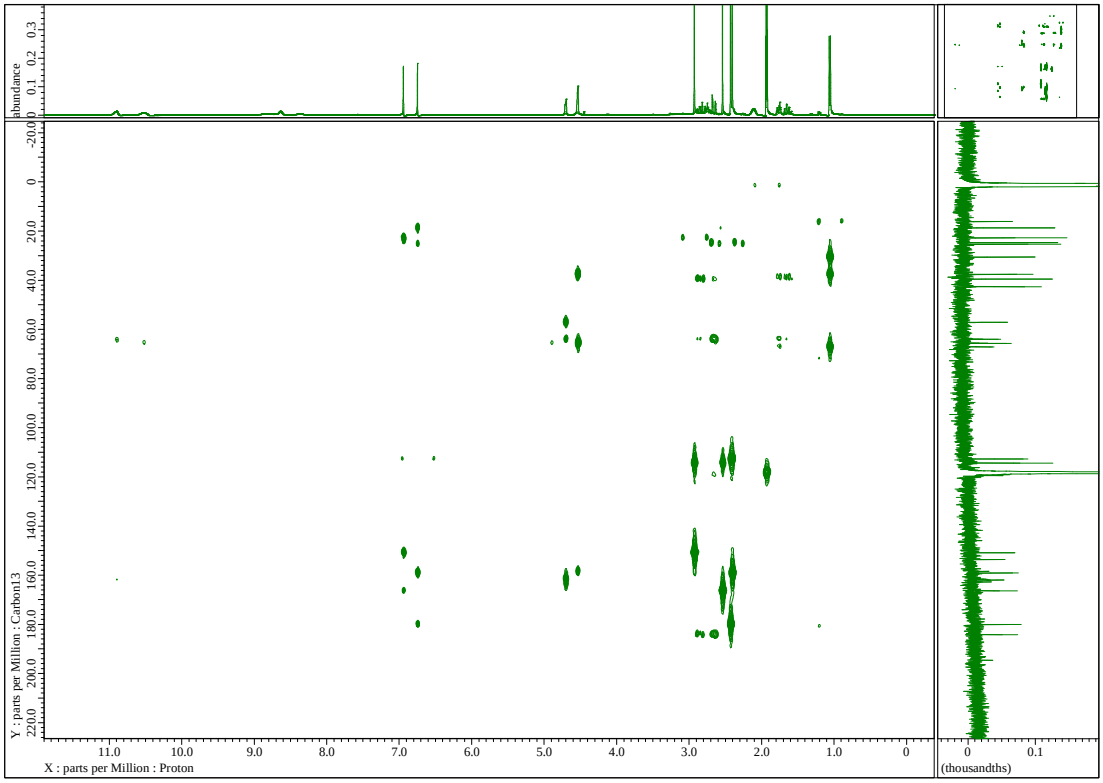

Figure S56. HMBC spectrum of compound **3** in CD_3CN-d_3 (400 MHz).

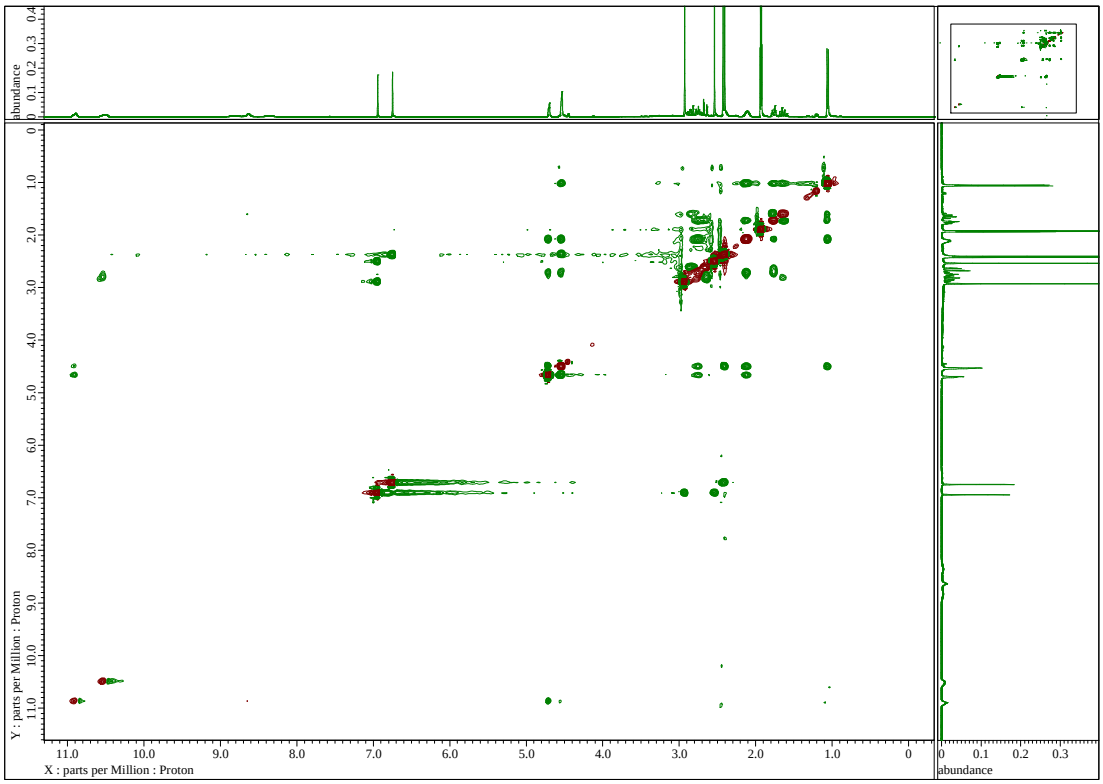

Figure S57. NOESY spectrum of compound **3** in CD_3CN-d_3 (400 MHz).

References

[1] CONFLEX 7, H. Goto, S. Obata, N. Nakayama, K. Ohta, CONFLEX Corporation, Tokyo, Japan, 2012.

[2] Gaussian 09, Revision C.01, M. J. Frisch, G. W. Trucks, H. B. Schlegel, G. E. Scuseria, M. A. Robb, J. R. Cheeseman, G. Scalmani, V. Barone, B. Mennucci, G. A. Petersson, H. Nakatsuji, M. Caricato, X. Li, H. P. Hratchian, A. F. Izmaylov, J. Bloino, G. Zheng, J. L. Sonnenberg, M. Hada, M. Ehara, K. Toyota, R. Fukuda, J. Hasegawa, M. Ishida, T. Nakajima, Y. Honda, O. Kitao, H. Nakai, T. Vreven, J. A. Montgomery, Jr., J. E. Peralta, F. Ogliaro, M. Bearpark, J. J. Heyd, E. Brothers, K. N. Kudin, V. N. Staroverov, R. Kobayashi, J. Normand, K. Raghavachari, A. Rendell, J. C. Burant, S. S. Iyengar, J. Tomasi, M. Cossi, N. Rega, J. M. Millam, M. Klene, J. E. Knox, J. B. Cross, V. Bakken, C. Adamo, J. Jaramillo, R. Gomperts, R. E. Stratmann, O. Yazyev, A. J. Austin, R. Cammi, C. Pomelli, J. W. Ochterski, R. L. Martin, K. Morokuma, V. G. Zakrzewski, G. A. Voth, P. Salvador, J. J. Dannenberg, S. Dapprich, A. D. Daniels, Ö. Farkas, J. B. Foresman, J. V. Ortiz, J. Cioslowski, and D. J. Fox, Gaussian, Inc., Wallingford CT, 2009.

[3] H. Kise, J. D. Reimer, *ZooKeys* **2016**, 49.

[4] R. Sakai, G. T. Swanson, K. Shimamoto, T. Green, A. Contractor, A. Ghetti, Y. Tamura-Horikawa, C. Oiwa, H. Kamiya, *J Pharmacol Exp Ther* **2001**, *296*, 650-658.